

# 1 **Circadian dynamics of the teleost skin immune-microbiome interface**

2

3 Amy R Ellison<sup>1</sup>, David Wilcockson<sup>2\*</sup> & Jo Cable<sup>3\*</sup>.

4 \* Joint senior authors, contributed equally.

5

6 1. School of Natural Sciences, Bangor University, Bangor, LL57 2DG, UK.

7 2. Institute of Biological, Environmental and Rural Sciences (IBERS), Aberystwyth University,

8 SY23 3DA, UK.

9 3. School of Biosciences, Cardiff University, Cardiff, CF10 3AX, UK.

10

11 **Keywords:** circadian rhythm, clock gene expression, microbiome, parasite infection, fish,  
12 aquaculture, photoperiod, immunity

13

## 14 **Abstract**

15 Circadian rhythms of host immune activity and their microbiomes are likely pivotal to health and  
16 disease resistance. The integration of chronotherapeutic approaches to disease mitigation in managed  
17 animals, however, is yet to be realised. In aquaculture, light manipulation is commonly used to  
18 enhance growth and control reproduction but may have unknown negative consequences for animal  
19 health. Infectious diseases are a major barrier to sustainable aquaculture and understanding the  
20 circadian dynamics of fish immunity and crosstalk with the microbiome is urgently needed. We  
21 demonstrate daily rhythms in fish skin immune expression and microbiomes, that are modulated by  
22 photoperiod and parasitic infection. We identify putative associations of host clock and immune gene  
23 profiles with microbial composition. Our results suggest circadian perturbation that shifts the  
24 magnitude and timing of immune and microbiota activity, is detrimental to fish health. This study  
25 represents a valuable foundation for investigating the utility of chronotherapies in aquaculture, and  
26 more broadly contributes to our understanding of circadian health in vertebrates.

27

## 28 **Introduction**

29 Circadian rhythms – endogenous daily cycles in physiological and behavioural processes – are a  
30 ubiquitous phenomenon to life. Living organisms are adapted to anticipate the daily variations in  
31 light, temperature, or food availability driven by the relentless 24 h rotation of Earth. Circadian  
32 rhythms are orchestrated by so-called “clock genes” driving transcriptional-translational  
33 autoregulatory feedback loops<sup>1</sup>, which are transduced to temporally coordinate biological activities.  
34 Immune functions are energetically costly<sup>2</sup> and often highly rhythmic, enabling organisms to mount  
35 their most efficient response at times when risk of infection or injury are highest<sup>3–5</sup>. Conversely,  
36 immune factors and infections can affect expression of molecular clocks<sup>6–8</sup> and subsequent rhythmic  
37 phenotypes<sup>9,10</sup>. Disruption of normal circadian cycles can impact immune functioning<sup>11,12</sup> and may  
38 increase disease risks<sup>13</sup>.

39 A primary function of immune systems is to protect the host from invading pathogenic  
40 microbes. However, animals are invariably colonized by a suite of microorganisms – their  
41 “microbiome” - which span the spectrum of symbiosis from mutualists to opportunistic pathogens.  
42 In vertebrates, it is increasingly apparent that immune systems and microbiomes are intricately linked,  
43 together mediating homeostasis and influencing disease outcomes<sup>14,15</sup>. Intriguingly, microbiomes  
44 may also be rhythmic, exhibiting diurnal fluctuations in community composition and activity<sup>16</sup>. In  
45 studies of the mammalian gut, it has been demonstrated that not only does expression of host clock  
46 genes shape microbiome rhythms<sup>17</sup>, but disruption of microbial rhythms in turn impacts host circadian  
47 functioning<sup>18</sup>.

48 Aquaculture is the world’s fastest growing food sector, but infectious disease is the principle  
49 barrier to sustainability<sup>19</sup> and a multi-billion-dollar problem for the global industry<sup>20</sup>. Whilst  
50 understanding of fish microbiomes is still in its infancy compared to mammalian systems, there is  
51 rapidly growing interest in their role for fish nutrition, health and disease resistance<sup>21–23</sup>. Photoperiod  
52 manipulation is commonly used in fish farms, with extended day lengths and, in the extreme, constant  
53 light, to promote increased growth rates, or control maturation and reproduction<sup>24–26</sup>. Fish are thought

54 to have a decentralised clock, with cells from multiple tissues expressing circadian genes<sup>27,28</sup>, self-  
55 sustained rhythmicity and light responsiveness (see<sup>29</sup> for review). In common with higher vertebrates,  
56 fish appear to exhibit circadian rhythmicity in certain immune factors<sup>27,28,30–33</sup>. Therefore, extreme  
57 lighting regimes may have profound implications for fish health and response to infection. Moreover,  
58 there are indications that infection and/or stress may impact expression of fish circadian clocks<sup>34,35</sup>.  
59 Currently, the extent to which light manipulation practices contribute to disease in aquaculture is  
60 unknown. More fundamentally, the daily dynamics of the fish immune-microbiome interface is yet  
61 to be explored. Uncovering the effects of infection and photoperiod on fish immune and microbiome  
62 rhythms will be pivotal for both aquaculture disease mitigation strategies, and a broader  
63 understanding of the role of holobiont chronobiological interactions for animal health.

64 Here, using rainbow trout (*Oncorhynchus mykiss*) as a model, we combine 16S rRNA  
65 metabarcoding and direct mRNA quantification methods to simultaneously characterise the circadian  
66 dynamics of skin clock and immune gene expression, and daily changes of skin microbiota. We  
67 compare circadian rhythms of host clock and immune gene expression and microbial community  
68 composition in healthy fish under regular light-dark cycles (12:12 LD) with those in fish  
69 experimentally infected with the ectoparasite crustacean *Argulus foliaceus* and/or raised under  
70 constant light (24:0 LD, hereafter LL). In addition, we assess rhythmicity in the functional potential  
71 of trout skin microbiomes and establish host expression-microbiome association networks.

72

## 73 **Results**

### 74 ***Photoperiod impacts host responses to infection***

75 Photoperiod (12:12 LD vs LL) had no significant impact on growth of juvenile rainbow trout over  
76 the 16-week trial period (weight:  $t_{956} = 0.073$ ,  $P = 0.942$ , length:  $t_{956} = 0.222$ ,  $P = 0.825$ ,  
77 Supplementary Figure 1a & 1b). However, a significantly higher number of *Argulus* lice survived 7  
78 days post-inoculation on fish maintained in constant light conditions ( $t_{115} = -8.418$ ,  $P = 1.23 \times 10^{-23}$ ,  
79 Supplementary Figure 1c). To examine overall immune responses to *Argulus* infection, we grouped  
80 fish from all timepoints, and contrasted expression of 27 genes from innate and adaptive immune

81 pathways between treatment groups (12:12 LD control, 12:12 LD infected, LL control, LL infected).  
82 Infected trout had significantly higher expression of 24 immune genes (89%) under 12:12 LD,  
83 whereas only 14 (52%) were significantly higher in infected fish compared to healthy controls under  
84 constant light (Figure 1). Two genes (*c3* and *tgfb*) were significantly reduced by infection in both light  
85 conditions (Figure 1). Expression levels were broadly similar among infected groups, although  
86 upregulation of the pro-inflammatory interleukins *il4* and *il6* was lower under constant light (Figure  
87 1). Conversely, comparisons of healthy (unchallenged) fish under LD and LL revealed a substantial  
88 difference in immune expression profiles, with unchallenged fish under constant light exhibiting  
89 elevated expression levels in 21 genes (78%), more similar to both infected groups in most immune  
90 genes (Figure 1).

#### 91 ***Circadian rhythmicity of host expression is altered by infection and photoperiod***

92 Under 12:12 LD, core and accessory vertebrate clock genes exhibited significant circadian  
93 rhythmicity in healthy trout skin (Figure 2, Table 1, Supplementary Figure 2). Many of these genes  
94 are also found to be expressed rhythmically in fish raised in constant light (Figure 2, Table 1,  
95 Supplementary Figure 2) and when fish are placed into “free-running” (DD) conditions  
96 (Supplementary Figure 3, Table 1). However, overall expression levels of clock genes are elevated in  
97 the absence of light cues (Figure 2, Supplementary Figure 2), except for *timeless* (suppressed  
98 expression in LL). In addition, *bmal2*, *clock1b*, *per1*, and *rora* exhibited a significantly different phase  
99 of expression in constant light (Table 1, Figure 2, Supplementary Figure 2).

100 *Argulus* lice infections had variable impacts on the expression levels and rhythmicity of the  
101 clock genes. When contrasted with healthy control groups, some gene rhythms were dampened in  
102 infected fish (i.e. significantly reduced amplitude; 12:12 LD *clock3*, LL *per1*), rendered arrhythmic  
103 (*cry2* in LL), and/or phase-shifted (*bmal1* in both light treatments, *cry1* and *per1* in 12:12 LD, *clock3*  
104 in LL). Rhythms of clock gene expression in infected fish under the two photoperiod treatments did  
105 not differ in amplitude. But, *bmal1*, *clock1b*, *clock3*, *cry1*, *per1*, *per2*, *rory* and *timeless* had  
106 significantly different phases of expression between infected fish under 12:12 LD and those raised in

107 constant light. In addition, *bmal2*, *clock3*, *csnk1d*, *per2*, *reverb* had increased rhythm mesors in LL,  
108 whilst *timeless* was suppressed (Table 1, Figure 2, Supplementary Figure 2).

109 Significant rhythmicity in expression was found in both innate and adaptive immune markers  
110 (Table 1, Supplementary Figures 4 & 5), with a substantial proportion remaining rhythmic under free-  
111 running (DD) conditions (Supplementary Figure 6). The cathelicidins (*cath1*, *cath2*), *igd*, *il17a*, and  
112 *tbx21*, while rhythmic in healthy fish under 12:12 LD, were arrhythmic in fish maintained in constant  
113 light (Table 1, Supplementary Figures 4 & 5). Of the immune genes rhythmic in healthy fish under  
114 both light conditions, the innate markers *chi*, *hamp* and *nos2*, and the adaptive markers *cd4*, *cd8a*,  
115 *foxp3b*, *igm*, *igt*, *tcrb* and *tgfb* had significantly different mesors; with the exception of *nos2*, all were  
116 more highly expressed in LL. However, some of these more highly expressed genes (*cd4*, *foxp3b*,  
117 *hamp*, *igt*, *tgfb*) and others with similar expression levels between photoperiods (*il4*, *tlr9*), were phase-  
118 shifted in constant light (Table 1, Supplementary Figures 4 & 5).

119 Fewer immune genes were rhythmically expressed in infected fish: 76% and 67% of rhythmic  
120 genes found in healthy fish were also rhythmic in the 12:12 LD and LL infected groups respectively.  
121 Under 12:12 LD, the vast majority (94%) of the immune genes assayed with rhythmicity in both  
122 healthy and infected fish exhibited higher mesors in the infected group. In contrast, only 57% of  
123 immune genes with rhythms in healthy and infected fish in LL had different expression levels (Table  
124 1). Only *tbx21* had a significantly altered amplitude in rhythm; with a higher amplitude in infected  
125 fish at 12:12 LD compared to both healthy 12:12 LD fish and infected fish in constant light. *Argulus*  
126 infection also shifted the phase of expression of *mhcii* under 12:12 LD and *c3*, *nos2* and *igt* in LL  
127 (Table 1).

### 128 ***Argulus* infection impacts skin mucus microbiome communities**

129 After read pre-processing, error correction, chimera removal, and filtering, a total of 1,037 amplified  
130 sequence variants (ASVs) were found across all samples. Rarefaction curves confirmed a minimum  
131 read depth of 2,000 was sufficient to reach saturation of diversity in trout skin (Supplementary Figure  
132 7a). Background water samples were distinct from fish groups (Supplementary Figure 7b) and had a

133 significantly higher alpha diversity (Supplementary Figure 7c). Contrasts of alpha diversity among  
134 fish samples revealed that the microbiomes of healthy fish under constant light were significantly less  
135 diverse than all other groups (Faith's PD, all pairwise Kruskal-Wallis tests  $P < 0.001$ , Supplementary  
136 Table 2). Multivariate permutational analysis of beta diversity indicated significant compositional  
137 differences among all groups (Supplementary Figure 7b, Supplementary Table 3).

138 The skin microbiome communities in all groups were dominated by *Proteobacteria*, with  
139 *Pseudomonadaceae* and *Burkholderiaceae* accounting for over 50% of the communities in all groups  
140 and timepoints (Figure 3). Wilcox rank-sum testing and DESeq2 both revealed substantial differences  
141 in the relative abundances of microbial taxa between healthy and lice-infected fish (Figure 4). At the  
142 higher taxonomic levels, healthy fish under both light treatments had a greater proportion of  
143 *Actinobacteria* and *Firmicutes* lineages, whilst both infected fish groups had increased *Bacterodia*  
144 lineages (Figure 4a). At the genus level, many *Gammaproteobacteria* were more abundant in both  
145 infected groups (e.g. *Aeromonas*, *Perluclidibaca*, *Undibacterium*, Figure 4b). *Bacteroidia* genera,  
146 including several *Chryseobacterium*, *Flectobacillus* and *Flavobacterium* ASVs were also increased  
147 in infected fish, with *Flavobacterium* accounting for some of the highest fold-changes in abundance  
148 (Figure 4b). Full lists of differentially abundant taxa are provided in Supplementary Table 4.

149 Functional prediction of microbiomes revealed putative differences in the activity of microbial  
150 communities among healthy and infected fish. LefSe analyses indicated pathways enriched in healthy  
151 fish groups were predominantly degradative classes including amino acid, aromatic compound, and  
152 carbohydrate degradation (Table 2). In contrast, functional enrichment of lice-infected fish  
153 microbiomes was dominated by biosynthetic pathways in both light conditions, particularly those  
154 involved in cofactor, carrier and vitamin biosynthesis (Table 2). Overall, a greater number of  
155 pathways were identified as differentially abundant between healthy and infected fish in LL,  
156 suggestive of a greater disruption in microbiota functional potential due to parasitic infection in fish  
157 maintained under constant light.

158 ***Circadian rhythmicity of skin microbiota and association with host gene expression***

159 Circadian rhythmicity in relative abundance was apparent in 49 skin bacteria genera in one or more  
160 of the treatment groups (Table 3, Figure 5). Of the 41 genera rhythmic in both healthy and infected  
161 fish at 12:12 LD, 17 (41.5%) had significantly different mesors. In contrast, 60.5% (23/38) had  
162 significantly different mesors when comparing healthy and infected fish under constant light.  
163 *Perlucidibaca*, *Undibacterium*, and *Rhodoferrax* had significantly greater rhythm amplitudes in  
164 infected fish under both light treatments. In addition, *Flectobacillus*, *Alkanibacter* and an unassigned  
165 *Burkholderiaceae* genus had higher rhythm amplitudes in infected 12:12 LD fish, whilst *Duganella*  
166 had higher amplitude in LL infected fish only. Under 12:12 LD, lice infection significantly altered  
167 rhythm phases of seven bacteria genera (Unknown *Rhizobiaceae*, Unknown *Rickettsiales*, *Deefgea*,  
168 *Massilia*, Unknown *Neisseriaceae*, Unknown *Chitinophagales* and *Legionella*). *Pseudoclavibacter*  
169 was the only genus found to have altered rhythm phase in LL healthy vs infected comparisons.

170 Visualisation of the timings of peak abundances of rhythmic taxa indicated no clear  
171 phylogenetic patterns (e.g. rhythmic *Proteobacteria* genera peak abundances were spread across the  
172 circadian cycle, Figure 5a). However, when considering the rhythms of the functional potential of the  
173 microbiome communities, we found evidence of temporal patterns (Figure 6). In healthy fish under  
174 12:12 LD, the majority of rhythmic biosynthetic (e.g. heme b, L-lysine and isoprene biosynthesis)  
175 and energy generation (e.g. glycolysis, TCA cycle) functions peaked in the first hours of light (ZT0-  
176 3), whilst degradation function peaks were found primarily in dark hours (ZT12-21). In contrast, in  
177 infected fish under 12:12 LD, rhythmic biosynthetic and energy generation functions predominantly  
178 peak in abundance towards the end of the dark period (ZT19-23), whilst degradation pathways peaked  
179 just before dark (ZT10-12). Constant light conditions also appeared to shift the broad temporal  
180 patterns of function abundances. In healthy fish under LL, many biosynthetic pathways (e.g. L-valine,  
181 heme b and enterobactin biosynthesis) peaked at ZT0-3, similar to the 12:12 LD group. However, we  
182 also found a large cluster of biosynthetic pathways peaking at ZT14-15 (e.g. fatty acid biosynthesis)  
183 and at ZT20-23 (spirilloxanthin and coenzyme M biosynthesis). In infected fish under LL,  
184 biosynthetic pathway rhythms were more dispersed, with peaks spread around the majority of the 24

185 h cycle. For degradation and generation of energy pathways in both healthy and infected fish under  
186 LL, we found multiple clusters of peak abundances around the 24 h cycle, rather than a single  
187 predominant cluster as in 12:12 LD conditions (Figure 6).

188 We used co-occurrence network analyses to assess associations of host gene expression and  
189 their microbiomes, using betweenness centrality scores and number of connections (degrees) to  
190 identify influential genes and bacteria genera<sup>36,37</sup>. In healthy 12:12 LD fish, there was a high level of  
191 connectivity within host immune and clock genes, and within microbial taxa (Figure 7). Links across  
192 the gene expression and bacteria subnetworks were primarily via the rhythmically expressed clock  
193 genes *clock1b*, *clock3*, *bmal1*, *rora*, and *csnk1d*. However, expression of the toll-like receptors *tlr2*  
194 and *tlr9* were significantly associated with abundance of *Bacillus* and *Enhydrobacter* respectively. In  
195 contrast, networks of infected fish under 12:12 LD revealed a higher level of connectivity between  
196 host expression and bacteria (Figure 7). The immune markers *cd4* and *tcrb*, and the clock gene *reverbb*  
197 were found to be most influential in terms of their betweenness centrality scores and number of  
198 significantly associated microbial taxa (Figure 7).

199 In contrast to 12:12 LD, clock genes were less influential (in terms of centrality) in gene-  
200 microbe networks for uninfected fish under constant light (Supplementary Figure 8). However,  
201 several immune genes (*igd*, *ifng*, *nos2*, *hamp*, *tcrb*, *foxp3b*) were significantly associated with one or  
202 more bacteria genera. *Tcrb* was most influential by betweenness centrality (expression positively  
203 correlated with *Janthinobacterium* and negatively with *Flavobacterium*), whilst *ifng* was linked to  
204 the highest number of taxa (*Escherichia-Shigella*, *Pseudomonas*, *Varioivorax*, *Stenotrophomonas* and  
205 *Pseudoclavibacter*). Similar to 12:12 LD contrasts, the network of infected fish under LL showed a  
206 higher level of connectivity between host gene expression and microbiota compared to the healthy  
207 network (Supplementary Figure 8), with the immune markers *cd8a* and *tcrb* found to be the most  
208 influential genes (in terms of number of associations with taxa and centrality score).

209

210 **Discussion**



211 We demonstrate the daily dynamics of immune expression and microbiome composition in fish skin  
212 and show ectoparasite infection and constant light – a commonly used environmental condition in  
213 aquaculture – can significantly alter circadian rhythms of immunity and microbiota, which may be  
214 detrimental for host disease resistance. In addition, we present association networks of host gene  
215 expression and their microbiomes, revealing clock expression and T cell populations are likely key  
216 in shaping the skin host-microbiome interface of teleosts. Our examination of the skin circadian  
217 immune response to infection under extreme photic regimes are directly relevant to fish culture  
218 practices; fish peripheral tissues are thought to have entrainable, light-responsive clocks<sup>29</sup>, which may  
219 make them particularly susceptible to negative health consequences from constant lighting as used in  
220 aquaculture.

221 Over our trial period, we found no significant difference in the growth of trout fry maintained  
222 under 12:12 LD and constant light (LL) when fish were provided equivalent food rations. However,  
223 when challenged with *Argulus* lice, their ability to clear infection was significantly altered by  
224 photoperiod. Under constant light, trout had a significantly higher lice burden 1 week after  
225 inoculation, indicating a reduced ability to mount an effective immune response. These findings are  
226 consistent with previous studies showing extended day length increases ectoparasite susceptibility  
227 and altered expression in specific immune genes in sticklebacks<sup>38</sup>. Immune profiles in uninfected fish  
228 showed elevated levels of expression in both innate and adaptive pathways under constant light. When  
229 infected with lice, trout under both photoperiods showed similar patterns of immune gene responses,  
230 except for the interleukins *il4* (mediator of Th2 differentiation) and *il6* (key to initiate inflammation)  
231 which were expressed at lower levels in constant light. Early inflammatory responses and subsequent  
232 initiation of Th2 processes are thought to be critical to resistance of crustacean ectoparasites in  
233 salmonids<sup>39</sup>. Taken together, chronic elevation of the immune gene expression – which may result in  
234 immune exhaustion<sup>40</sup> or other immunopathologies<sup>41</sup> – and reduced ability to mount effective  
235 responses key to lice resistance suggest rearing of fish in the absence of light cues are likely to be  
236 detrimental for health.

237           The impact of photoperiod on overall magnitude of immune gene activation is not be the only  
238 factor important to parasite resistance; the rhythmicity and the appropriate timing of immune activity  
239 (i.e. when fish are maximally vulnerable to pathogen attack) may also be key to pathogen defences.  
240 Under regular light-dark cycles, we show trout skin is highly rhythmic in expression of the core  
241 vertebrate clock genes and many immune genes in both innate and adaptive pathways. In essence, we  
242 find the highest expression of pro-inflammatory markers (e.g. *il6*, *il17a*) at the onset of the light period  
243 and peaks in anti-microbial peptide genes (e.g. cathelicidins) mid-light phase, whilst immunoglobulin  
244 and T cell markers were highest during dark hours. The timing of different facets of immune systems,  
245 typically peaks of inflammatory mechanisms during active phases and pathways of repair and  
246 infection resolution during resting phases, are considered to have evolved to offer hosts greatest  
247 protection from invading pathogens when most likely to encounter them, whilst avoiding  
248 energetically inefficient and potentially immunopathological risk of continual immune activation<sup>42</sup>.  
249 We found that constant light resulted in arrhythmic expression of genes involved in mucosa anti-  
250 microbial (e.g. cathelicidins, *igd*, *il17a*) and Th1 (*tbx21*) responses. Furthermore, genes with phase-  
251 shifted expression rhythms in constant light were dominated by those involved in T cell differentiation  
252 and regulation (e.g. *cd4*, *foxp3b*, *il4*, *tgfb*). Loss of synchrony between host immunity and parasite  
253 activity and/or immune evasion rhythms are very likely to be detrimental for host fitness and  
254 survival<sup>43</sup>. Our results indicate that this is a factor in the reduced clearance of lice in fish reared in  
255 constant light. Clearly, the impacts of light cycle perturbation, be it intentional such as in aquaculture  
256 or unintentionally due to light pollution<sup>44</sup>, must be more carefully considered for animal health.

257           The primary function of fish skin mucus is as a protective barrier and hosts diverse  
258 communities of microbes<sup>45</sup> which are thought to contribute to protection from microbial pathogens  
259 via competitive and/or antagonistic activities<sup>46,47</sup>. While pathogenic taxa occur mostly at low levels  
260 in healthy teleost microbiomes, their proliferation is a common signal of microbiome perturbation  
261 and dysbiosis<sup>48</sup>. *Argulus* lice infestations are commonly observed alongside bacterial, fungal or viral  
262 infections<sup>49</sup>. Here, we demonstrate significant reorganisation of bacterial communities and their

263 potential functional activities in trout skin when infected with *A. foliaceus*, including notable  
264 increases in abundance of genera associated with infectious disease<sup>50,51</sup>. Fish lice may elicit host  
265 immune profiles and/or destabilize skin microbiota communities resulting in reduced “colonization  
266 resistance”<sup>48</sup>, or be direct vectors<sup>52,53</sup>. Further research into the microbiota of *Argulus* and other fish  
267 ectoparasites, and their pathogen vectoring capabilities, will be valuable for understanding their role  
268 in coinfection dynamics. Intriguingly, trout raised in constant light had a significantly lower  
269 microbiome diversity and, when challenged with *Argulus*, exhibited greater shifts in both taxonomic  
270 composition and functional potential compared to fish under regular light-dark regimes. Given the  
271 growing body of evidence for the importance of “healthy” microbial communities<sup>54</sup> for effective host  
272 homeostasis and disease resistance<sup>55,56</sup>, characterising circadian disruption to microbiomes is  
273 important for understanding animal disease risks.

274 We demonstrate significant daily dynamicity in the skin microbiome of trout; a substantial  
275 proportion of bacteria genera exhibit rhythmic changes in relative abundance, suggesting a temporal  
276 structure to microbiome functional activity. Parasitic infection appears to perturb microbiome  
277 composition, and shift the timings of peak biosynthetic, degradative and energy generation pathway  
278 activity in the microbial community. Understanding of the functional importance to the host of  
279 commensal microbiota in teleost skin is still in its infancy<sup>48</sup>, and predictive metagenomic analyses  
280 are only indicative of actual microbial activity<sup>57</sup>. Temporal metatranscriptomic profiling will be an  
281 important means to build upon our results to decipher the functional significance of teleost mucosal  
282 microbiota and their daily coordination of activity. Nevertheless, as interest builds towards the utility  
283 of microbiome engineering strategies to promote health and productivity in aquaculture<sup>23,48,58</sup>, we  
284 propose that a chronobiological understanding of fish microbiomes may be crucial for their  
285 effectiveness. The daily rhythms of both fish host immunity and their microbiome communities, for  
286 example, could be critical to uptake and establishment of probiotics treatments. Chronotherapeutics  
287 – the timed application of treatments and vaccines<sup>59</sup> – in human medicine holds great promise for  
288 improving efficacies but is yet to be given full consideration for managed animal health.

289 In the mammalian gut – by far the most studied host-microbiome interface – there is a complex  
290 interplay between immune factors that shape microbial communities and, conversely, microbiota  
291 profoundly affecting immune system development and maintenance<sup>14,15</sup>. Mammal gut microbiome  
292 daily rhythms may themselves play a role in host circadian health<sup>60,61</sup>. However, in other tissues, and  
293 particularly for non-mammalian vertebrates, host immune-microbiome connectivity and circadian  
294 dynamics remains poorly understood. For teleosts, there is evidence that macrophages<sup>62</sup> and adaptive  
295 immune components (e.g. T cells<sup>63</sup> and immunoglobulins<sup>64</sup>) may be key to mucosal microbiome  
296 composition. Our study is the first to present an integrated analysis of skin microbiomes with a broad  
297 set of immune and circadian clock gene expression profiles in fish. We found genes of the core  
298 secondary feedback loops (e.g. *bmal*, *clock*, *rora*, *csnk1d*) that define the vertebrate molecular clock  
299 to be strongly associated with microbial taxa relative abundances in uninfected trout under 12:12 LD,  
300 yet these direct clock-microbe associations were largely absent in constant light. Similarly, mice  
301 faecal microbiota composition appears closely linked to *bmall*, with knock-outs resulting in  
302 arrhythmicity and altered abundance of microbial taxa<sup>17</sup>. Our results suggest this arm of the biological  
303 clock may be pivotal to orchestrating changes in mucosal microbiomes across vertebrates. However,  
304 we also find perturbation of microbial communities via ectoparasite infection reconfigures the  
305 connectivity of host expression and microbiota. In LL and LD conditions, lice infected fish immune-  
306 microbe networks show a greater level of connectivity between host immune gene expression and  
307 microbial taxa compared to uninfected individuals. In particular, our results indicate T cell markers  
308 to be central to this host-microbiome interface during ectoparasite infection. Under 12:12 LD, we  
309 find the T helper cell gene *cd4* to be strongly linked to microbiome composition, whilst in constant  
310 light the cytotoxic T cell marker *cd8a* appears to be more influential to microbiome-immune  
311 associations. For teleost fish, the ratios and distributions of T cell populations are not well defined<sup>65,66</sup>,  
312 although CD4+ and CD8+ subsets appear to have different roles in pathogen defence<sup>67</sup>. Our results  
313 suggest their relative importance to shaping fish mucosal microbiomes, or vice versa, warrant further  
314 investigation. Disentangling the directionality of the associations we find via controlled

315 manipulations of host immune cell populations, clock gene expression, and microbiota will  
316 undoubtedly be key to advancing the concept of circadian holobiont health.

317 Our study demonstrates the complex daily interaction of fish immune expression and  
318 microbiomes, which are impacted by photoperiod and infection status. There is rapidly growing  
319 recognition for the detrimental impacts of circadian rhythm perturbation in human medicine<sup>13</sup>, though  
320 little attention has been paid to the implications for animal health. In an industry that heavily utilises  
321 light manipulation, contemporary aquaculture practices may be significantly exacerbating current  
322 disease issues. We provide here an important resource for furthering efforts to integrate chronobiology  
323 into animal disease mitigation strategies. In addition, as artificial light at night (i.e. light pollution)  
324 encroaches on ever greater proportions of the world's ecosystems<sup>68</sup>, it is vital studies such as ours are  
325 considered for the implications on health and disease dynamics in wild populations.

326

## 327 **Methods**

### 328 *Experimental design and sample collection*

329 Juvenile female triploid rainbow trout fry (*O. mykiss*, 10 days post-yolk sac absorption, n = 500) were  
330 obtained from a commercial hatchery (Bibury Trout Farm, UK). Fry were visually and  
331 microscopically determined free of parasitic infections upon arrival and maintained in a re-circulating  
332 aquaculture system (RAS) in Cardiff University (water temperature  $12 \pm 0.5$  °C, pH  $7.5 \pm 0.2$ ). The  
333 trout were randomly assigned to duplicate tanks (45 x 60 x 60 cm, 150 L) under one of two  
334 photoperiod conditions; 12:12 LD (lights on at zeitgeber time 0; ZT0, off at ZT12) or 24:0 LD  
335 (constant light, LL). Each tank was individually illuminated with a full-spectrum white LED bar (80  
336 lux at surface) and surrounded with blackout material to ensure no disturbance from ambient light.  
337 Fish were fed with a commercial trout feed (Nutraparr, Skretting, UK) *ad libitum* at ZT2-3 and ZT9-  
338 10 daily. Water oxygen saturation (>90%), ammonia (<0.02 mg/L), nitrite (<0.01 mg L<sup>-1</sup>) and nitrate  
339 (<15 mg L<sup>-1</sup>) were maintained within an appropriate range.

340 After one month acclimation to light conditions, 130 fish from each light treatment were  
341 individually isolated in 1 L plastic containers. Half of the fish from each light treatment (n = 65 per  
342 treatment) were individually inoculated with ten *Argulus foliaceus* metanauplii (24 hrs post-hatching).  
343 *Argulus* metanauplii were obtained from eggs of wild-caught adult pairs (sourced from Risca Canal,  
344 Newport), maintained at Cardiff University. Egg strings were collected and hatched under laboratory  
345 conditions according to Stewart et al. (2018). Inoculations were performed at ZT4-5. Fish were  
346 individually held in a glass container with 50 ml of tank water and 10 metanauplii added. Fish were  
347 observed until all lice had attached (within 2 minutes) and then returned to their 1 L container. Control  
348 fish (those not inoculated with *Argulus* lice) were also held for 2 min in 50 ml of water to control for  
349 handling stress. Water in all individual containers were changed daily, feeding continued on schedule  
350 outlined above, and light conditions maintained at same intensity, spectrum and duration as during  
351 acclimation period. The remaining fish were maintained in the RAS system. Once a week, 30 random  
352 fish per light treatment were weighed (g) and measured (standard length, SL in cm) for 16 weeks to  
353 monitor growth rates. General linear models of standard length and weight, including photoperiod  
354 and sampling day, were used to assess differences in growth between light treatments. All procedures  
355 were performed under Home Office project license PPL 303424 with full approval of Cardiff  
356 University Animal Ethics committee.

357 One week after inoculation, sampling of fish was performed over a 48 h period to encompass  
358 two full circadian cycles. Starting at ZT0 (lights on in 12:12 LD treatment), every 4 h, five fish from  
359 each condition (12:12 LD control, 12:12 LD *Argulus*-infected, LL control, LL *Argulus*-infected) were  
360 euthanised using an overdose of tricaine methanesulfonate (MS222, 500 mg L<sup>-1</sup>) according to Home  
361 Office Schedule 1. At timepoints during dark periods in 12:12 LD treatment, fish were handled and  
362 euthanised in dim red light. Immediately after euthanasia, infected fish were visually inspected to  
363 quantify number of lice surviving and the lice removed to ensure they were not included in tissue  
364 samples. Welch's two sample T test was used to determine difference in infection load (number of  
365 *Argulus*) between light treatments. All sampled fish were weighed (g) and measured (standard length,

366 SL in cm). Skin swabs (MWE MW-100) were rubbed along the entire lateral body surface five times  
367 each side and immediately frozen at -80 C to preserve skin mucus microbiota for DNA extraction.  
368 All skin from immediately posterior to opercula to the caudal peduncle was dissected using sterile  
369 forceps, preserved in RNAlater (Invitrogen), and stored at -80 C until RNA extraction. All dissections  
370 for each timepoint were performed within an 1 hour window. At each timepoint-treatment  
371 combination, 10 ml of water from all containers was pooled and frozen at -80°C to provide  
372 background controls for skin microbiome analyses. To test for endogenous expression rhythms, an  
373 additional 65 uninfected fish maintained at 12:12 LD were individually isolated and held in constant  
374 darkness (DD). After 24 h, starting at ZT0, five fish every 4 h were sampled as above.

### 375 ***RNA extraction, gene expression quantification and analyses***

376 Total RNA was individually extracted from each skin sample using RNeasy Mini kits (Qiagen). RNA  
377 was quantified using Qubit Broad Range RNA assays (ThermoFisher Scientific). mRNA expression  
378 patterns in the skin were measured by Nanostring analysis, following manufacturer's guidelines, at  
379 Liverpool Centre for Genomic Research. The nCounter PlexSet oligonucleotide and probe design was  
380 performed at NanoString Technologies (NanoString Technologies) for 48 genes, including four  
381 housekeeping genes (Supplementary Table S1). The oligonucleotide probes were synthesized at  
382 Integrated DNA Technologies. Titration reactions were performed according to supplier's instructions  
383 with RNA inputs between 250 ng and 700 ng to determine the required RNA amount for hybridization  
384 reaction. 600 ng total RNA per sample was used for PlexSet hybridization reaction for 20 h according  
385 to manufacturer's instructions.

386 Samples were processed on a nCounter MAX prep station (NanoString Technologies) and  
387 cartridges were scanned in a generation II nCounter Digital Analyzer (NanoString Technologies).  
388 RCC files (nCounter data files) were used for data analysis. RCC files were imported into the  
389 NanoString nSolver 4.0 analysis software and raw data pre-processing and normalization was  
390 performed according to manufacturer's instructions for standard procedures (positive normalization  
391 to geomean of top 3 positive controls, codeset content normalization using housekeeping genes *hpert1*,

392 *polr1b*, *polr2i* and codeset calibration with the reference sample). The housekeeping gene *rplp0* and  
393 *aanat2* expression were not detected and excluded from analyses.

394 To assess overall differences in immune responses to infection under the different light  
395 treatments, pairwise t-tests comparing normalised expression of immune genes were performed in R  
396 (version 4.0.3). To detect rhythmicity in expression of clock and immune genes, empirical JTK Cycle  
397 (eJTK\_cycle<sup>69</sup>) analyses were applied with a set period of 24 h, a phase search every 4 h from ZT0  
398 to ZT20, and an asymmetry search every 4 h from ZT4 to ZT20. FDR-corrected empirical p-values  
399 less than 0.1 were considered moderately rhythmic<sup>70-72</sup>, and less than 0.05 strongly rhythmic.  
400 CircaCompare<sup>31</sup> was used to estimate rhythmic genes' peak expression time, mesor and amplitude,  
401 and to statistically contrast rhythms.

#### 402 ***DNA extraction, 16S rRNA gene amplification, Illumina sequencing and analyses***

403 DNA was extracted from skin swabs using Qiagen DNeasy Blood and Tissue kits according to <sup>73</sup> to  
404 maximise lysis of microbiome community and DNA recovery. PCR amplification of the 16S rRNA  
405 V4 region, using 515F and 806R primers, was performed in triplicate for each DNA extract, pooled  
406 and prepared for Illumina MiSeq sequencing according to <sup>74</sup>. Gel electrophoresis was used to estimate  
407 concentrations for pooling individual amplicon libraries. Negative controls for extractions and PCR,  
408 and mock community positive controls were included for sequencing. Libraries were sequenced using  
409 a 2 x 250 bp Illumina MiSeq run at the Cardiff Biosciences Genomics Hub.

410 Paired-end demultiplexed Illumina sequencing reads were imported into the Quantitative  
411 Insights Into Microbial Ecology 2 (QIIME2<sup>75</sup>). Sequences were then quality filtered, dereplicated,  
412 chimeras identified and paired-end reads merged in QIIME2 using DADA2 with default settings.  
413 Classification of Amplicon Sequence Variants (ASVs) was performed using a Naïve Bayes algorithm  
414 trained using sequences representing the bacterial V4 rRNA region available from the SILVA database  
415 (<https://www.arb-silva.de/download/archive/qiime>; Silva\_132), and the corresponding taxonomic  
416 classifications were obtained using the q2-feature-classifier plugin in QIIME2. The classifier was  
417 then used to assign taxonomic information to representative sequences of each ASV. Following



418 rarefaction analysis, samples with less than 2000 sequences were excluded from further analyses.  
419 QIIME2 was used to analyse alpha (Kruskal-Wallis pairwise tests of Faith's phylogenetic distance)  
420 and beta (pairwise PERMANOVA) diversity measures. ASVs were filtered to exclude those assigned  
421 to eukaryotes or eukaryotic organelles and include ones with at least 100 copies in at least two  
422 samples. The QIIME2 output data were imported in RStudio (Version 1.3.959) with the Bioconductor  
423 package phyloseq<sup>76</sup>, for subsetting, normalizing, and plotting of the data.

424 Differential abundance of ASVs between healthy and infected fish in both light treatments  
425 were determined using DESeq2<sup>77</sup>, with FDR-corrected p-values less than 0.05 considered significant.  
426 Differential abundances of all taxonomic levels were also determined and visualised using  
427 MicrobiomeAnalyst<sup>78</sup> heat trees using default settings. We inferred the microbial gene content from  
428 the taxa abundance using PICRUSt2<sup>79</sup>. We used LefSe analyses to identify group differences in the  
429 inferred gene abundance of MetaCyc pathways, using the online galaxy server  
430 (<https://huttenhower.sph.harvard.edu/galaxy/>). LDA scores >2.0 were considered significant.  
431 Rhythmicity of microbial genera and MetaCyc pathway abundances were determined following the  
432 same methods as gene expression (see above). To determine potential associations of host gene  
433 expression and the microbiome, Spearman correlation tests were performed including only genera  
434 found in at least 50% of samples in each treatment group. Corrected p-values (using qvalue R  
435 package) of less than 0.05 were considered significantly correlated. Correlation networks were  
436 visualised using gephi<sup>80</sup> and influential nodes determined using degree centrality scores and number  
437 of connections (degrees).

438

### 439 **Acknowledgments**

440 This study was funded by a BBSRC Discovery Fellowship awarded to AE (BB/R010609/1). We thank  
441 Liverpool Centre for Genomic Research and Cardiff Biosciences Genome Hub for their assistance in  
442 data generation. We also thank members of the Cable research group for their assistance in animal  
443 husbandry.

444 **References**

- 445 1. Dunlap, J. C. Molecular bases for circadian clocks. *Cell* **96**, 271–290 (1999).
- 446 2. Lochmiller, R. L. & Deerenberg, C. Trade-offs in evolutionary immunology: Just what is the  
447 cost of immunity? *Oikos* **88**, 87–98 (2000).
- 448 3. Wang, W. *et al.* Timing of plant immune responses by a central circadian regulator. *Nature*  
449 **470**, 110–114 (2011).
- 450 4. Scheiermann, C., Kunisaki, Y. & Frenette, P. S. Circadian control of the immune system. *Nat.*  
451 *Rev. Immunol.* **13**, 190–198 (2013).
- 452 5. Curtis, A. M., Bellet, M. M., Sassone-Corsi, P. & O’Neill, L. A. J. Circadian clock proteins  
453 and immunity. *Immunity* **40**, 178–186 (2014).
- 454 6. Okada, K. *et al.* Injection of LPS causes transient suppression of biological clock genes in  
455 rats. *J. Surg. Res.* **145**, 5–12 (2008).
- 456 7. Cavadini, G. *et al.* TNF- $\alpha$  suppresses the expression of clock genes by interfering with E-  
457 box-mediated transcription. *Proc. Natl. Acad. Sci.* **104**, 12843–12848 (2007).
- 458 8. de Leone, M. J. *et al.* Bacterial Infection Disrupts Clock Gene Expression to Attenuate  
459 Immune Responses. *Curr. Biol.* (2020).
- 460 9. Shirasu-Hiza, M. M., Dionne, M. S., Pham, L. N., Ayres, J. S. & Schneider, D. S. Interactions  
461 between circadian rhythm and immunity in *Drosophila melanogaster*. *Curr. Biol.* **17**, R353–  
462 R355 (2007).
- 463 10. Marpegán, L., Bekinschtein, T. A., Costas, M. A. & Golombek, D. A. Circadian responses to  
464 endotoxin treatment in mice. *J. Neuroimmunol.* **160**, 102–109 (2005).
- 465 11. Castanon-Cervantes, O. *et al.* Dysregulation of inflammatory responses by chronic circadian  
466 disruption. *J. Immunol.* **185**, 5796–5805 (2010).
- 467 12. Adams, K. L., Castanon-Cervantes, O., Evans, J. A. & Davidson, A. J. Environmental  
468 circadian disruption elevates the IL-6 response to lipopolysaccharide in blood. *J. Biol.*  
469 *Rhythms* **28**, 272–277 (2013).

- 470 13. Touitou, Y., Reinberg, A. & Touitou, D. Association between light at night, melatonin  
471 secretion, sleep deprivation, and the internal clock: Health impacts and mechanisms of  
472 circadian disruption. *Life Sci.* **173**, 94–106 (2017).
- 473 14. Thaiss, C. A., Zmora, N., Levy, M. & Elinav, E. The microbiome and innate immunity.  
474 *Nature* **535**, 65 (2016).
- 475 15. McDermott, A. J. & Huffnagle, G. B. The microbiome and regulation of mucosal immunity.  
476 *Immunology* **142**, 24–31 (2014).
- 477 16. Zarrinpar, A., Chaix, A., Yooseph, S. & Panda, S. Diet and feeding pattern affect the diurnal  
478 dynamics of the gut microbiome. *Cell Metab.* **20**, 1006–1017 (2014).
- 479 17. Liang, X., Bushman, F. D. & FitzGerald, G. A. Rhythmicity of the intestinal microbiota is  
480 regulated by gender and the host circadian clock. *Proc. Natl. Acad. Sci.* **112**, 10479–10484  
481 (2015).
- 482 18. Leone, V. *et al.* Effects of diurnal variation of gut microbes and high-fat feeding on host  
483 circadian clock function and metabolism. *Cell Host Microbe* **17**, 681–689 (2015).
- 484 19. Stentiford, G. D. *et al.* New paradigms to help solve the global aquaculture disease crisis.  
485 *PLoS Pathog.* **13**, e1006160 (2017).
- 486 20. Lafferty, K. D. *et al.* Infectious diseases affect marine fisheries and aquaculture economics.  
487 (2015).
- 488 21. Tarnecki, A. M., Burgos, F. A., Ray, C. L. & Arias, C. R. Fish intestinal microbiome:  
489 diversity and symbiosis unravelled by metagenomics. *J. Appl. Microbiol.* **123**, 2–17 (2017).
- 490 22. Ghanbari, M., Kneifel, W. & Domig, K. J. A new view of the fish gut microbiome: advances  
491 from next-generation sequencing. *Aquaculture* **448**, 464–475 (2015).
- 492 23. Perry, W. B., Lindsay, E., Payne, C. J., Brodie, C. & Kazlauskaitė, R. The role of the gut  
493 microbiome in sustainable teleost aquaculture. *Proc. R. Soc. B* **287**, 20200184 (2020).
- 494 24. Biswas, A. K., Seoka, M., Tanaka, Y., Takii, K. & Kumai, H. Effect of photoperiod  
495 manipulation on the growth performance and stress response of juvenile red sea bream

- 496           (*Pagrus major*). *Aquaculture* **258**, 350–356 (2006).
- 497   25.   Rad, F., Bozaoğlu, S., Gözükar, S. E., Karahan, A. & Kurt, G. Effects of different long-day  
498       photoperiods on somatic growth and gonadal development in Nile tilapia (*Oreochromis*  
499       *niloticus* L.). *Aquaculture* **255**, 292–300 (2006).
- 500   26.   Berrill, I. K., Porter, M. J. R., Smart, A., Mitchell, D. & Bromage, N. R. Photoperiodic  
501       effects on precocious maturation, growth and smoltification in Atlantic salmon, *Salmo salar*.  
502       *Aquaculture* **222**, 239–252 (2003).
- 503   27.   Onoue, T., Nishi, G., Hikima, J., Sakai, M. & Kono, T. Circadian oscillation of TNF- $\alpha$  gene  
504       expression regulated by clock gene, BMAL1 and CLOCK1, in the Japanese medaka (*Oryzias*  
505       *latipes*). *Int. Immunopharmacol.* **70**, 362–371 (2019).
- 506   28.   Zhang, P., Yu, C. & Sun, L. Japanese flounder (*Paralichthys olivaceus*) Bmal1 is involved in  
507       the regulation of inflammatory response and bacterial infection. *Aquaculture* 735330 (2020).
- 508   29.   Frøland Steindal, I. A. & Whitmore, D. Circadian clocks in fish—what have we learned so  
509       far? *Biology (Basel)*. **8**, 17 (2019).
- 510   30.   Binuramesh, C. & Michael, R. D. Diel variations in the selected serum immune parameters in  
511       *Oreochromis mossambicus*. *Fish Shellfish Immunol.* **30**, 824–829 (2011).
- 512   31.   Ángeles Esteban, M., Cuesta, A., Rodríguez, A. & Meseguer, J. Effect of photoperiod on the  
513       fish innate immune system: a link between fish pineal gland and the immune system. *J.*  
514       *Pineal Res.* **41**, 261–266 (2006).
- 515   32.   Lazado, C. C., Skov, P. V. & Pedersen, P. B. Innate immune defenses exhibit circadian  
516       rhythmicity and differential temporal sensitivity to a bacterial endotoxin in Nile tilapia  
517       (*Oreochromis niloticus*). *Fish Shellfish Immunol.* **55**, 613–622 (2016).
- 518   33.   Taira, G., Onoue, T., Hikima, J., Sakai, M. & Kono, T. Circadian clock components Bmal1  
519       and Clock1 regulate tlr9 gene expression in the Japanese medaka (*Oryzias latipes*). *Fish*  
520       *Shellfish Immunol.* **105**, 438–445 (2020).
- 521   34.   Ellison, A. R. *et al.* Transcriptomic response to parasite infection in Nile tilapia (*Oreochromis*

- 522 *niloticus*) depends on rearing density. *BMC Genomics* **19**, 723 (2018).
- 523 35. Ellison, A. R. *et al.* Comparative transcriptomics reveal conserved impacts of rearing density  
524 on immune response of two important aquaculture species. *Fish Shellfish Immunol.* (2020).
- 525 36. Greer, R., Dong, X., Morgun, A. & Shulzhenko, N. Investigating a holobiont: Microbiota  
526 perturbations and transkingdom networks. *Gut Microbes* **7**, 126–135 (2016).
- 527 37. Greenblum, S., Turnbaugh, P. J. & Borenstein, E. Metagenomic systems biology of the  
528 human gut microbiome reveals topological shifts associated with obesity and inflammatory  
529 bowel disease. *Proc. Natl. Acad. Sci.* **109**, 594–599 (2012).
- 530 38. Whiting, J. R., Mahmud, M. A., Bradley, J. E. & MacColl, A. D. C. Prior exposure to long-  
531 day photoperiods alters immune responses and increases susceptibility to parasitic infection  
532 in stickleback. *Proc. R. Soc. B* **287**, 20201017 (2020).
- 533 39. Braden, L. M., Koop, B. F. & Jones, S. R. M. Signatures of resistance to *Lepeophtheirus*  
534 *salmonis* include a TH2-type response at the louse-salmon interface. *Dev. Comp. Immunol.*  
535 **48**, 178–191 (2015).
- 536 40. Saeidi, A. *et al.* T-cell exhaustion in chronic infections: reversing the state of exhaustion and  
537 reinvigorating optimal protective immune responses. *Front. Immunol.* **9**, 2569 (2018).
- 538 41. Graham, A. L., Allen, J. E. & Read, A. F. Evolutionary causes and consequences of  
539 immunopathology. *Annu. Rev. Ecol. Evol. Syst.* 373–397 (2005).
- 540 42. Westwood, M. L. *et al.* The evolutionary ecology of circadian rhythms in infection. *Nat.*  
541 *Ecol. Evol.* **3**, 552–560 (2019).
- 542 43. Reece, S. E., Prior, K. F. & Mideo, N. The life and times of parasites: rhythms in strategies  
543 for within-host survival and between-host transmission. *J. Biol. Rhythms* **32**, 516–533  
544 (2017).
- 545 44. Longcore, T. & Rich, C. Ecological light pollution. *Front. Ecol. Environ.* **2**, 191–198 (2004).
- 546 45. Ross, A. A., Hoffmann, A. R. & Neufeld, J. D. The skin microbiome of vertebrates.  
547 *Microbiome* **7**, 1–14 (2019).

- 548 46. Pérez-Sánchez, T. *et al.* Identification and characterization of lactic acid bacteria isolated  
549 from rainbow trout, *Oncorhynchus mykiss* (Walbaum), with inhibitory activity against  
550 *Lactococcus garvieae*. *J. Fish Dis.* **34**, 499–507 (2011).
- 551 47. Balcázar, J. L. *et al.* In vitro competitive adhesion and production of antagonistic compounds  
552 by lactic acid bacteria against fish pathogens. *Vet. Microbiol.* **122**, 373–380 (2007).
- 553 48. Llewellyn, M. S., Boutin, S., Hoseinifar, S. H. & Derome, N. Teleost microbiomes: the state  
554 of the art in their characterization, manipulation and importance in aquaculture and fisheries.  
555 *Roles Mech. Parasit. Aquat. Microb. Communities* 109 (2015).
- 556 49. Walker, P. D., Flik, G. & Bonga, S. E. W. The biology of parasites from the genus *Argulus*  
557 and a review of the interactions with its host. *Host-Parasite Interact.* **55**, 107–129 (2004).
- 558 50. Adikesavalu, H., Patra, A., Banerjee, S., Sarkar, A. & Abraham, T. J. Phenotypic and  
559 molecular characterization and pathology of *Flectobacillus roseus* causing flectobacillosis in  
560 captive held carp *Labeo rohita* (Ham.) fingerlings. *Aquaculture* **439**, 60–65 (2015).
- 561 51. Loch, T. P. & Faisal, M. Emerging flavobacterial infections in fish: a review. *J. Adv. Res.* **6**,  
562 283–300 (2015).
- 563 52. Jakob, E., Barker, D. E. & Garver, K. A. Vector potential of the salmon louse *Lepeophtheirus*  
564 *salmonis* in the transmission of infectious haematopoietic necrosis virus (IHNV). *Dis. Aquat.*  
565 *Organ.* **97**, 155–165 (2011).
- 566 53. Ahne, W. *Argulus foliaceus* L. and *Piscicola geometra* L. as mechanical vectors of spring  
567 viraemia of carp virus (SVCV). *J. Fish Dis.* **8**, 241–242 (1985).
- 568 54. Lloyd-Price, J., Abu-Ali, G. & Huttenhower, C. The healthy human microbiome. *Genome*  
569 *Med.* **8**, 1–11 (2016).
- 570 55. Harris, E. V, de Roode, J. C. & Gerardo, N. M. Diet–microbiome–disease: Investigating  
571 diet’s influence on infectious disease resistance through alteration of the gut microbiome.  
572 *PLoS Pathog.* **15**, e1007891 (2019).
- 573 56. Cani, P. D. *et al.* Microbial regulation of organismal energy homeostasis. *Nat. Metab.* **1**, 34–

- 574 46 (2019).
- 575 57. Fiore, C. L., Jarett, J. K., Steinert, G. & Lesser, M. P. Trait-Based Comparison of Coral and  
576 Sponge Microbiomes. *Sci. Rep.* **10**, 1–16 (2020).
- 577 58. Pérez-Sánchez, T., Ruiz-Zarzuela, I., de Blas, I. & Balcázar, J. L. Probiotics in aquaculture: a  
578 current assessment. *Rev. Aquac.* **6**, 133–146 (2014).
- 579 59. Ballesta, A., Innominato, P. F., Dallmann, R., Rand, D. A. & Lévi, F. A. Systems  
580 chronotherapeutics. *Pharmacol. Rev.* **69**, 161–199 (2017).
- 581 60. Pearson, J. A., Wong, F. S. & Wen, L. Cross talk between circadian rhythms and the  
582 microbiota. *Immunology* (2020).
- 583 61. Gibbs, J. E. & Butler, T. D. Circadian host-microbiome interactions in immunity. *Front.*  
584 *Immunol.* **11**, 1783 (2020).
- 585 62. Earley, A. M., Graves, C. L. & Shiau, C. E. Critical role for a subset of intestinal  
586 macrophages in shaping gut microbiota in adult zebrafish. *Cell Rep.* **25**, 424–436 (2018).
- 587 63. Brugman, S. *et al.* T lymphocytes control microbial composition by regulating the abundance  
588 of *Vibrio* in the zebrafish gut. *Gut Microbes* **5**, 737–747 (2014).
- 589 64. Xu, Z. *et al.* Specialization of mucosal immunoglobulins in pathogen control and microbiota  
590 homeostasis occurred early in vertebrate evolution. *Sci. Immunol.* **5**, (2020).
- 591 65. Takizawa, F. *et al.* The expression of CD8 $\alpha$  discriminates distinct T cell subsets in teleost  
592 fish. *Dev. Comp. Immunol.* **35**, 752–763 (2011).
- 593 66. Kelly, C. & Salinas, I. Under pressure: interactions between commensal microbiota and the  
594 teleost immune system. *Front. Immunol.* **8**, 559 (2017).
- 595 67. Sukeda, M. *et al.* Innate cell-mediated cytotoxicity of CD8<sup>+</sup> T cells against the protozoan  
596 parasite *Ichthyophthirius multifiliis* in the ginbuna crucian carp, *Carassius auratus*  
597 *langsdorfii*. *Dev. Comp. Immunol.* **115**, 103886 (2020).
- 598 68. Hölker, F. *et al.* The dark side of light: a transdisciplinary research agenda for light pollution  
599 policy. *Ecol. Soc.* **15**, (2010).

- 600 69. Hutchison, A. L. *et al.* Improved statistical methods enable greater sensitivity in rhythm  
601 detection for genome-wide data. *PLoS Comput Biol* **11**, e1004094 (2015).
- 602 70. Wang, Y. *et al.* A proteomics landscape of circadian clock in mouse liver. *Nat. Commun.* **9**,  
603 1–16 (2018).
- 604 71. Lafaye, G., Desterke, C., Marulaz, L. & Benyamina, A. Cannabidiol affects circadian clock  
605 core complex and its regulation in microglia cells. *Addict. Biol.* **24**, 921–934 (2019).
- 606 72. Cui, P. *et al.* Identification of human circadian genes based on time course gene expression  
607 profiles by using a deep learning method. *Biochim. Biophys. Acta (BBA)-Molecular Basis*  
608 *Dis.* **1864**, 2274–2283 (2018).
- 609 73. Gill, C., van de Wiggert, J. H. H. M., Blow, F. & Darby, A. C. Evaluation of lysis methods for  
610 the extraction of bacterial DNA for analysis of the vaginal microbiota. *PLoS One* **11**,  
611 e0163148 (2016).
- 612 74. Caporaso, J. G. *et al.* Ultra-high-throughput microbial community analysis on the Illumina  
613 HiSeq and MiSeq platforms. *ISME J.* **6**, 1621–1624 (2012).
- 614 75. Bolyen, E. *et al.* Reproducible, interactive, scalable and extensible microbiome data science  
615 using QIIME 2. *Nat. Biotechnol.* **37**, 852–857 (2019).
- 616 76. McMurdie, P. J. & Holmes, S. phyloseq: an R package for reproducible interactive analysis  
617 and graphics of microbiome census data. *PLoS One* **8**, e61217 (2013).
- 618 77. Love, M. I., Huber, W. & Anders, S. Moderated estimation of fold change and dispersion for  
619 RNA-Seq data with DESeq2. *Genome Biol.* **15**, 550 (2014).
- 620 78. Dhariwal, A. *et al.* MicrobiomeAnalyst: a web-based tool for comprehensive statistical,  
621 visual and meta-analysis of microbiome data. *Nucleic Acids Res.* **45**, W180–W188 (2017).
- 622 79. Douglas, G. M. *et al.* PICRUSt2 for prediction of metagenome functions. *Nat. Biotechnol.* 1–  
623 5 (2020).
- 624 80. Bastian, M., Heymann, S. & Jacomy, M. Gephi: an open source software for exploring and  
625 manipulating networks. in *Proceedings of the International AAAI Conference on Web and*



626            *Social Media* vol. 3 (2009).

627

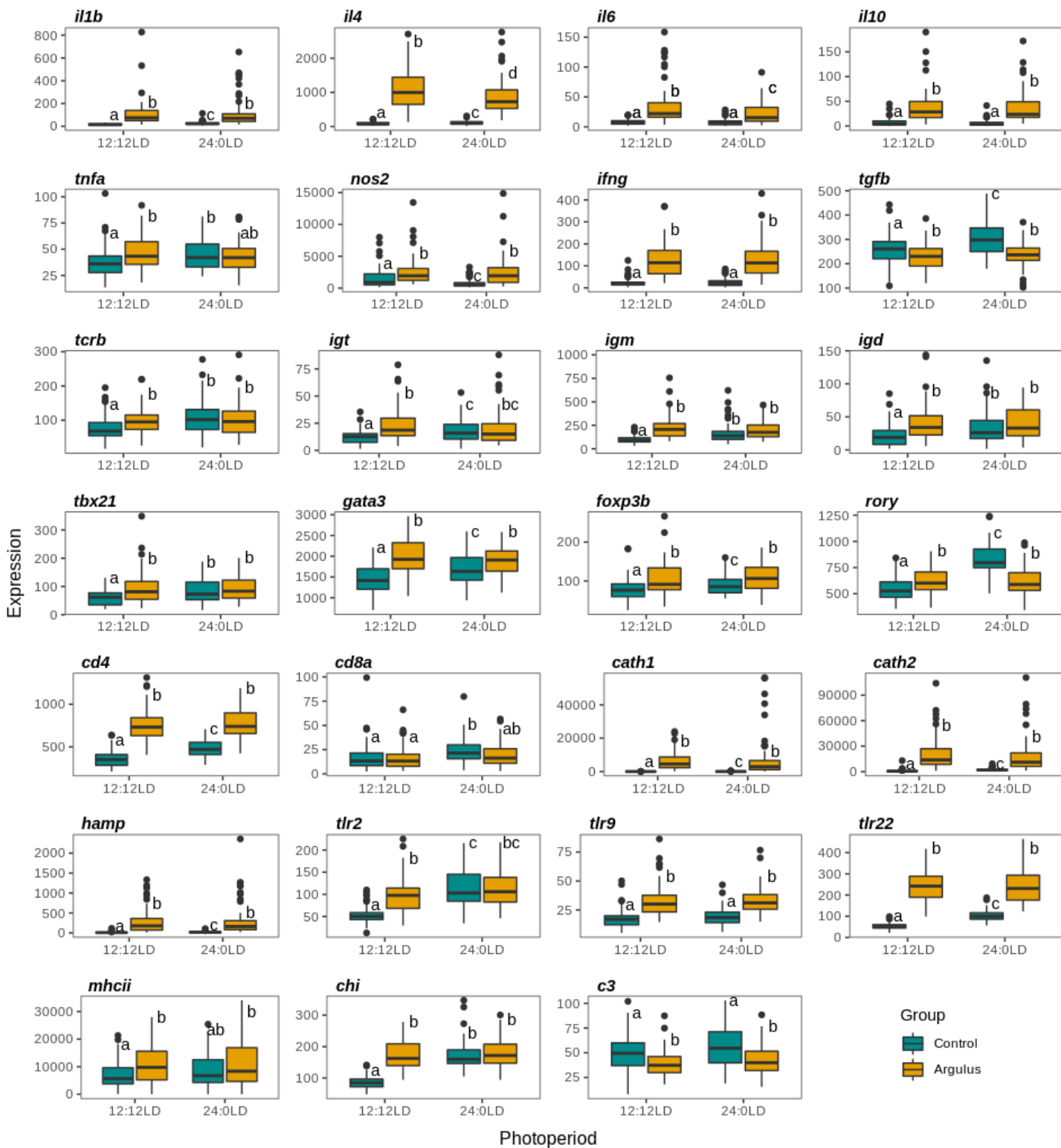
628



635 **Table 2:** Results of LefSe analyses to identify group differences in the inferred gene abundance of  
 636 MetaCyc pathways.  
 637

Superclass	Class	Pathway	Group	Log10 LDA Score	Corrected P-value
<b>Control vs Argulus 12:12 LD</b>					
Biosynthesis	Carbohydrate Biosynthesis	dTDP-L-rhamnose biosynthesis	Argulus	2.03	1.07E-04
Biosynthesis	Carbohydrate Biosynthesis	CMP-3-deoxy-D-manno-oxulosonate biosynthesis	Argulus	2.11	1.34E-07
Biosynthesis	Cell Structure Biosynthesis	Lipid IVA biosynthesis	Argulus	2.09	1.55E-08
Biosynthesis	Cell Structure Biosynthesis	Kds transfer to lipid IVA III	Argulus	2.13	6.53E-08
Biosynthesis	Cofactor, Carrier, and Vitamin Biosynthesis	Pyridoxal 5-phosphate biosynthesis I	Argulus	2.05	1.71E-04
Biosynthesis	Cofactor, Carrier, and Vitamin Biosynthesis	Thiamine salvage II	Argulus	2.07	1.51E-08
Biosynthesis	Cofactor, Carrier, and Vitamin Biosynthesis	Thiazole biosynthesis I	Argulus	2.08	4.66E-02
Biosynthesis	Cofactor, Carrier, and Vitamin Biosynthesis	Biotin biosynthesis I	Argulus	2.17	5.96E-05
Biosynthesis	Cofactor, Carrier, and Vitamin Biosynthesis	NAD salvage pathway III	Argulus	2.26	6.41E-04
Biosynthesis	Cofactor, Carrier, and Vitamin Biosynthesis	Thiamine diphosphate biosynthesis I	Argulus	2.31	3.08E-02
Biosynthesis	Nucleoside and Nucleotide Biosynthesis	Pyrimidine ribonucleotides de novo biosynthesis	Argulus	2.00	2.44E-08
Biosynthesis	Nucleoside and Nucleotide Biosynthesis	Pyrimidine nucleosides salvage	Argulus	2.01	9.04E-07
Biosynthesis	Nucleoside and Nucleotide Biosynthesis	UMP biosynthesis I	Argulus	2.01	1.85E-08
Biosynthesis	Other Biosynthesis	8-amino-7-oxononanoate biosynthesis I	Argulus	2.08	3.68E-04
Biosynthesis	Other Biosynthesis	Geranyl diphosphate biosynthesis II	Argulus	2.04	2.08E-04
Biosynthesis	Secondary Metabolite Biosynthesis	PreQ0 biosynthesis	Argulus	2.00	1.64E-03
Degradation/Utilization/Assimilation	Amino Acid Degradation	L-leucine degradation I	Argulus	2.06	1.34E-04
Degradation/Utilization/Assimilation	Other Degradation/Utilization/Assimilation	Octane oxidation	Argulus	2.38	5.11E-03
Macromolecule Modification	Nucleic Acid Processing	Queuosine biosynthesis I	Argulus	2.01	1.17E-08
Biosynthesis	Cofactor, Carrier, and Vitamin Biosynthesis	Heme b biosynthesis from glycine	Control	2.13	1.50E-03
Biosynthesis	Fatty Acid and Lipid Biosynthesis	Palmitate biosynthesis II	Control	2.48	3.95E-02
Biosynthesis	Secondary Metabolite Biosynthesis	Enterobactin biosynthesis	Control	2.00	1.91E-03
Degradation/Utilization/Assimilation	Amino Acid Degradation	L-histidine degradation I	Control	2.18	3.78E-02
Degradation/Utilization/Assimilation	Aromatic Compound Degradation	Phenylacetate degradation I (aerobic)	Control	2.02	3.48E-03
Degradation/Utilization/Assimilation	Aromatic Compound Degradation	4-methylcatechol degradation	Control	2.21	2.17E-03
Degradation/Utilization/Assimilation	Aromatic Compound Degradation	Salicylate degradation	Control	2.22	8.00E-04
Degradation/Utilization/Assimilation	Aromatic Compound Degradation	Toluene degradation III (aerobic)	Control	2.37	4.87E-04
Degradation/Utilization/Assimilation	Aromatic Compound Degradation	Protocatechuate degradation II	Control	2.49	2.64E-02
Degradation/Utilization/Assimilation	Carbohydrate Degradation	Sucrose degradation II (sucrose invertase)	Control	2.14	2.13E-02
Degradation/Utilization/Assimilation	Carbohydrate Degradation	Glycogen degradation I	Control	2.15	1.16E-02
Degradation/Utilization/Assimilation	Carbohydrate Degradation	Starch degradation V	Control	2.17	1.76E-02
Degradation/Utilization/Assimilation	Carbohydrate Degradation	Ketoglucuronate metabolism	Control	2.13	8.87E-03
Degradation/Utilization/Assimilation	Inorganic Nutrient Metabolism	Urea cycle	Control	2.16	8.99E-03
Degradation/Utilization/Assimilation	Secondary Metabolite Biosynthesis	4-deoxy-L-threo-hex-4-enopyranuronate degradation	Control	2.08	2.62E-03
Degradation/Utilization/Assimilation	Secondary Metabolite Degradation	Anhydromuropeptides recycling I	Control	2.15	6.25E-03
Generation of Precursor Metabolites and Energy	Fermentation	Mixed acid fermentation	Control	2.20	8.65E-03
Generation of Precursor Metabolites and Energy	Penitose Phosphate Pathways	Penitose phosphate pathway	Control	2.14	1.83E-02
<b>Control vs Argulus 24:0 LD</b>					
Biosynthesis	Amine and Polyamine Biosynthesis	Arginine and polyamine biosynthesis	Argulus	2.16	7.89E-03
Biosynthesis	Amine and Polyamine Biosynthesis	Polyamine biosynthesis I	Argulus	2.15	3.37E-03
Biosynthesis	Amino Acid Biosynthesis	L-alanine biosynthesis	Argulus	2.12	1.44E-06
Biosynthesis	Amino Acid Biosynthesis	L-glutamate and L-glutamine biosynthesis	Argulus	2.12	4.84E-02
Biosynthesis	Amino Acid Biosynthesis	L-threonine biosynthesis	Argulus	2.16	4.80E-11
Biosynthesis	Amino Acid Biosynthesis	S-adenosyl-L-methionine cycle I	Argulus	2.15	3.24E-02
Biosynthesis	Aromatic Compound Biosynthesis	Chromistatol metabolism	Argulus	2.15	1.20E-03
Biosynthesis	Carbohydrate Biosynthesis	CMP-3-deoxy-D-manno-oxulosonate biosynthesis	Argulus	2.15	1.92E-07
Biosynthesis	Carbohydrate Biosynthesis	UDP-glucose-derived O-antigen building blocks biosynthesis	Argulus	2.23	5.25E-08
Biosynthesis	Cell Structure Biosynthesis	Kds transfer to lipid IVA III	Argulus	2.19	3.50E-08
Biosynthesis	Cell Structure Biosynthesis	Lipid IVA biosynthesis	Argulus	2.13	1.93E-09
Biosynthesis	Cofactor, Carrier, and Vitamin Biosynthesis	2-carboxy-1,4-naphthoquinol biosynthesis	Argulus	2.02	5.79E-03
Biosynthesis	Cofactor, Carrier, and Vitamin Biosynthesis	Biotin biosynthesis I	Argulus	2.36	1.69E-06
Biosynthesis	Cofactor, Carrier, and Vitamin Biosynthesis	Demethylmenaquinol-6 biosynthesis I	Argulus	2.16	4.56E-04
Biosynthesis	Cofactor, Carrier, and Vitamin Biosynthesis	Demethylmenaquinol-8 biosynthesis I	Argulus	2.16	3.22E-02
Biosynthesis	Cofactor, Carrier, and Vitamin Biosynthesis	Demethylmenaquinol-9 biosynthesis	Argulus	2.16	4.72E-04
Biosynthesis	Cofactor, Carrier, and Vitamin Biosynthesis	Heme b biosynthesis I (aerobic)	Argulus	2.03	8.90E-06
Biosynthesis	Cofactor, Carrier, and Vitamin Biosynthesis	Heme b biosynthesis II (oxygen-independent)	Argulus	2.07	2.04E-06
Biosynthesis	Cofactor, Carrier, and Vitamin Biosynthesis	Menaquinol-10 biosynthesis	Argulus	2.26	4.56E-04
Biosynthesis	Cofactor, Carrier, and Vitamin Biosynthesis	Menaquinol-11 biosynthesis	Argulus	2.23	4.56E-04
Biosynthesis	Cofactor, Carrier, and Vitamin Biosynthesis	Menaquinol-12 biosynthesis	Argulus	2.23	1.39E-03
Biosynthesis	Cofactor, Carrier, and Vitamin Biosynthesis	Menaquinol-13 biosynthesis	Argulus	2.23	1.39E-03
Biosynthesis	Cofactor, Carrier, and Vitamin Biosynthesis	Menaquinol-6 biosynthesis I	Argulus	2.26	4.56E-04
Biosynthesis	Cofactor, Carrier, and Vitamin Biosynthesis	Menaquinol-7 biosynthesis	Argulus	2.23	9.35E-04
Biosynthesis	Cofactor, Carrier, and Vitamin Biosynthesis	Menaquinol-8 biosynthesis I	Argulus	2.26	1.19E-03
Biosynthesis	Cofactor, Carrier, and Vitamin Biosynthesis	Menaquinol-9 biosynthesis	Argulus	2.26	1.19E-03
Biosynthesis	Cofactor, Carrier, and Vitamin Biosynthesis	NAD de novo biosynthesis I (from aspartate)	Argulus	2.04	1.46E-02
Biosynthesis	Cofactor, Carrier, and Vitamin Biosynthesis	Phylloquinol biosynthesis	Argulus	2.02	6.58E-03
Biosynthesis	Cofactor, Carrier, and Vitamin Biosynthesis	Thiamine diphosphate biosynthesis I	Argulus	2.68	7.99E-06
Biosynthesis	Cofactor, Carrier, and Vitamin Biosynthesis	Thiamine diphosphate biosynthesis II	Argulus	2.32	2.13E-02
Biosynthesis	Cofactor, Carrier, and Vitamin Biosynthesis	Thiamine salvage II	Argulus	2.09	4.03E-08
Biosynthesis	Cofactor, Carrier, and Vitamin Biosynthesis	Thiazole biosynthesis I	Argulus	2.53	1.20E-05
Biosynthesis	Cofactor, Carrier, and Vitamin Biosynthesis	Thiazole biosynthesis II (aerobic bacteria)	Argulus	2.10	2.81E-02
Biosynthesis	Fatty Acid and Lipid Biosynthesis	(5Z)-dodecenoate biosynthesis I	Argulus	2.08	1.43E-04
Biosynthesis	Fatty Acid and Lipid Biosynthesis	(Kdo)2-lipid A biosynthesis	Argulus	2.55	5.92E-04
Biosynthesis	Fatty Acid and Lipid Biosynthesis	cis-vaccinate biosynthesis	Argulus	2.31	4.92E-07
Biosynthesis	Fatty Acid and Lipid Biosynthesis	Fatty acid elongation (saturated)	Argulus	2.08	8.79E-04
Biosynthesis	Fatty Acid and Lipid Biosynthesis	Oleate biosynthesis IV (anaerobic)	Argulus	2.08	1.41E-03
Biosynthesis	Fatty Acid and Lipid Biosynthesis	Palmitoleate biosynthesis I	Argulus	2.10	6.79E-04
Biosynthesis	Nucleoside and Nucleotide Biosynthesis	Purine nucleotides de novo biosynthesis II	Argulus	2.39	7.67E-03
Biosynthesis	Nucleoside and Nucleotide Biosynthesis	Pyrimidine deoxyribonucleotides de novo biosynthesis II	Argulus	2.31	1.15E-02
Biosynthesis	Nucleoside and Nucleotide Biosynthesis	Pyrimidine ribonucleotides salvage	Argulus	2.22	4.18E-04
Biosynthesis	Other Biosynthesis	8-amino-7-oxononanoate biosynthesis I	Argulus	2.22	7.58E-05
Degradation/Utilization/Assimilation	Amino Acid Degradation	Histidine, purine & pyrimidine biosynthesis	Argulus	2.12	2.13E-02
Degradation/Utilization/Assimilation	Aromatic Compound Degradation	Protocatechuate degradation I (meta-cleavage pathway)	Argulus	2.09	3.41E-07
Degradation/Utilization/Assimilation	Carbohydrate Degradation	D-galactose degradation I (Leloir pathway)	Argulus	2.16	4.57E-03
Degradation/Utilization/Assimilation	Nucleoside and Nucleotide Degradation	Pyrimidine deoxyribonucleotides degradation	Argulus	2.18	1.19E-02
Generation of Precursor Metabolites and Energy	Fermentation	Acetylethyl degradation (anaerobic)	Argulus	2.43	6.12E-04
Generation of Precursor Metabolites and Energy	Fermentation	Pyruvate fermentation to acetate and lactate II	Argulus	2.18	6.96E-03
Generation of Precursor Metabolites and Energy	TCA cycle	TCA cycle IV	Argulus	2.18	6.86E-03
Generation of Precursor Metabolites and Energy	TCA cycle	TCA cycle V	Argulus	2.21	6.04E-03
Macromolecule Modification	Nucleic Acid Processing	tRNA processing	Argulus	2.08	1.60E-03
Biosynthesis	Amine and Polyamine Biosynthesis	Cocaine biosynthesis	Control	2.04	3.03E-05
Biosynthesis	Amine and Polyamine Biosynthesis	Polyamine biosynthesis II	Control	2.14	1.15E-02
Biosynthesis	Amino Acid Biosynthesis	L-arginine biosynthesis III (via N-acetyl-L-citrulline)	Control	2.06	1.74E-02
Biosynthesis	Amino Acid Biosynthesis	L-serine and glycine biosynthesis I	Control	2.14	1.41E-03
Biosynthesis	Carbohydrate Biosynthesis	Coaric acid building blocks biosynthesis	Control	2.42	1.58E-03
Biosynthesis	Carbohydrate Biosynthesis	GDP-mannose biosynthesis	Control	2.18	6.29E-03
Biosynthesis	Carbohydrate Biosynthesis	GDP-mannose-derived O-antigen building blocks biosynthesis	Control	2.46	2.06E-03
Biosynthesis	Carbohydrate Biosynthesis	UDP-N-acetylglucosamine-derived O-antigen building blocks biosynthesis	Control	2.21	1.61E-02
Biosynthesis	Cell Structure Biosynthesis	Peptidoglycan biosynthesis IV	Control	2.21	3.47E-04
Biosynthesis	Cofactor, Carrier, and Vitamin Biosynthesis	Cob(II)yrinate a,c-diamide biosynthesis II	Control	2.33	2.30E-03
Biosynthesis	Cofactor, Carrier, and Vitamin Biosynthesis	Heme b biosynthesis from glycine	Control	2.33	2.78E-05
Biosynthesis	Cofactor, Carrier, and Vitamin Biosynthesis	NAD de novo biosynthesis II (from tryptophan)	Control	2.11	1.44E-02
Biosynthesis	Fatty Acid and Lipid Biosynthesis	Fatty acid biosynthesis initiation	Control	2.11	1.15E-02
Degradation/Utilization/Assimilation	Amino Acid Degradation	L-histidine degradation I	Control	2.35	1.10E-03
Degradation/Utilization/Assimilation	Amino Acid Degradation	L-histidine degradation II	Control	2.42	2.26E-03
Degradation/Utilization/Assimilation	Amino Acid Degradation	L-tryptophan degradation	Control	2.00	1.44E-02
Degradation/Utilization/Assimilation	Amino Acid Degradation	L-tyrosine degradation I	Control	2.36	4.03E-03
Degradation/Utilization/Assimilation	Aromatic Compound Degradation	3-phenylpropionate degradation	Control	2.08	1.93E-02
Degradation/Utilization/Assimilation	Aromatic Compound Degradation	4-hydroxyphenylacetate degradation	Control	2.07	3.22E-03
Degradation/Utilization/Assimilation	Aromatic Compound Degradation	4-methylcatechol degradation (ortho cleavage)	Control	2.45	1.34E-05
Degradation/Utilization/Assimilation	Aromatic Compound Degradation	Aromatic compounds degradation via β-ketoadipate	Control	2.40	6.23E-04
Degradation/Utilization/Assimilation	Aromatic Compound Degradation	Catechol degradation III (ortho-cleavage pathway)	Control	2.40	6.23E-04
Degradation/Utilization/Assimilation	Aromatic Compound Degradation	Catechol degradation to β-ketoadipate II	Control	2.17	6.35E-07
Degradation/Utilization/Assimilation	Aromatic Compound Degradation	Catechol degradation to β-ketoadipate	Control	2.39	1.08E-03
Degradation/Utilization/Assimilation	Aromatic Compound Degradation	Phenylacetate degradation I (aerobic)	Control	2.14	4.60E-03
Degradation/Utilization/Assimilation	Aromatic Compound Degradation	Protocatechuate degradation II	Control	2.80	3.20E-04
Degradation/Utilization/Assimilation	Aromatic Compound Degradation	Salicylate degradation	Control	2.48	7.96E-07
Degradation/Utilization/Assimilation	Aromatic Compound Degradation	Toluene degradation III (aerobic)	Control	2.64	2.07E-07
Degradation/Utilization/Assimilation	Carbohydrate Degradation	Glucose and glucose-1-phosphate degradation	Control	2.16	3.16E-02
Degradation/Utilization/Assimilation	Carbohydrate Degradation	Glucose and xylose degradation	Control	2.18	4.07E-02
Degradation/Utilization/Assimilation	Carbohydrate Degradation	Glycogen degradation I	Control	2.19	2.98E-04
Degradation/Utilization/Assimilation	Carbohydrate Degradation	Starch degradation V	Control	2.22	9.04E-04
Degradation/Utilization/Assimilation	Carbohydrate Degradation	Sucrose degradation III (sucrose invertase)	Control	2.15	5.16E-03
Degradation/Utilization/Assimilation	Carbohydrate Degradation	Ketoglucuronate metabolism	Control	2.45	3.08E-05
Degradation/Utilization/Assimilation	Inorganic Nutrient Metabolism	Methylphosphonate degradation I	Control	2.36	2.56E-03
Degradation/Utilization/Assimilation	Inorganic Nutrient Metabolism	Urea cycle	Control	2.42	1.35E-04
Degradation/Utilization/Assimilation	Nucleoside and Nucleotide Degradation	Adenosine nucleotides degradation II	Control	2.39	3.89E-02
Degradation/Utilization/Assimilation	Nucleoside and Nucleotide Degradation	Guanosine nucleotides degradation III	Control	2.32	2.99E-02
Degradation/Utilization/Assimilation	Secondary Metabolite Biosynthesis	myo-, chiro- & scylo-inositol degradation	Control	2.16	3.06E-03
Degradation/Utilization/Assimilation	Secondary Metabolite Biosynthesis	myo-inositol degradation I	Control	2.48	9.04E-04
Degradation/Utilization/Assimilation	Secondary Metabolite Degradation	Anhydromuropeptides recycling I	Control	2.27	3.51E-02
Detoxification	Antibiotic Resistance	Polymyxin resistance	Control	2.18	9.17E-03
Generation of Precursor Metabolites and Energy	Fermentation	Pyruvate fermentation to isobutanol	Control	2.33	4.18E-05
Generation of Precursor Metabolites and Energy	Penitose Phosphate Pathways	Penitose phosphate pathway	Control	2.43	1.28E-04
Generation of Precursor Metabolites and Energy	Photosynthesis	Photosynthesis	Control	2.16	7.74E-02
Generation of Precursor Metabolites and Energy	TCA cycle	TCA cycle VI	Control	2.60	9.82E-04
Generation of Precursor Metabolites and Energy	TCA cycle	TCA cycle VII	Control	2.57	9.98E-04





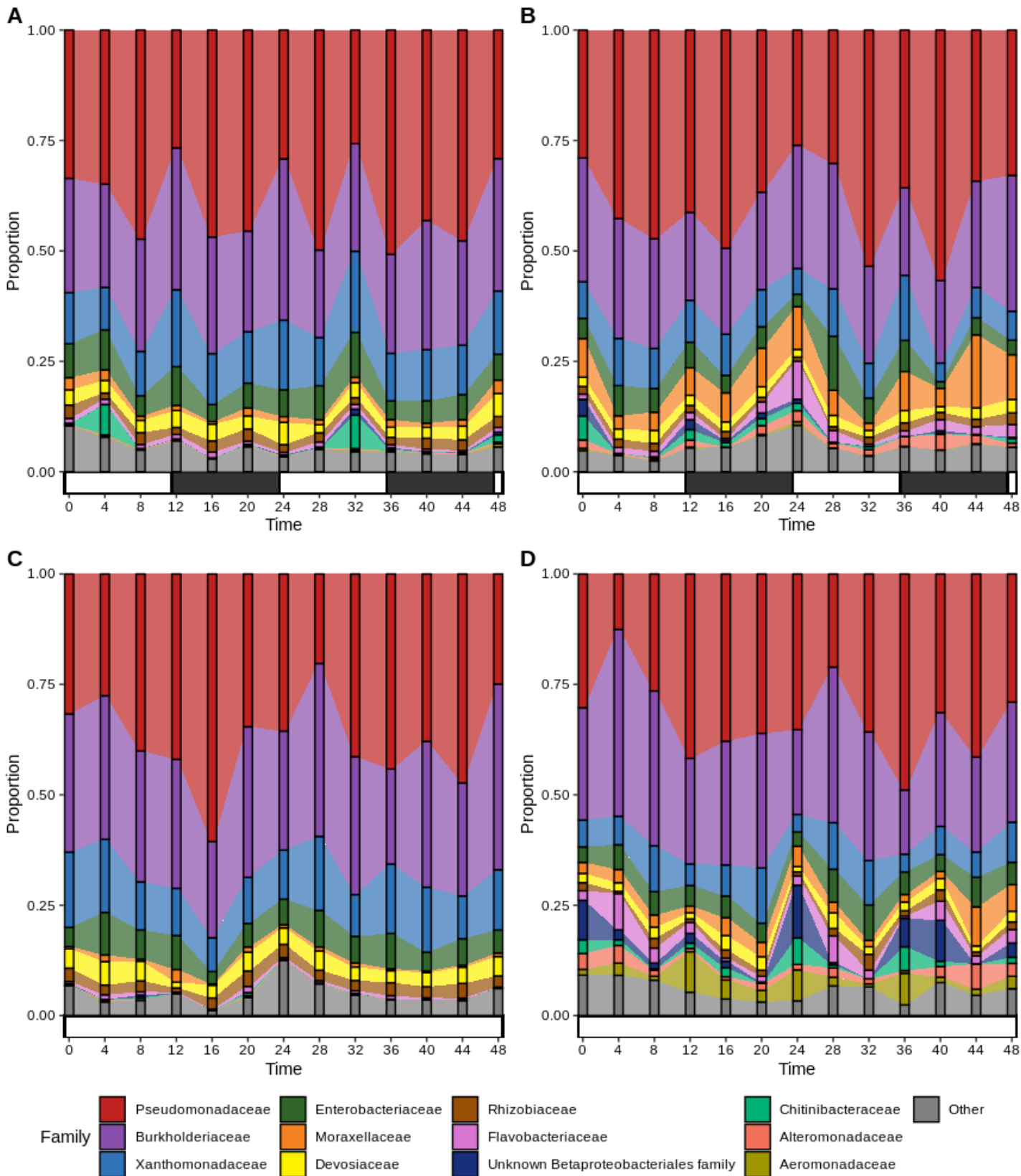
644

645 **Figure 1:** Expression of immune genes in uninfected (control; cyan) and *Argulus*-infected (orange)  
 646 rainbow trout maintained under 12:12 LD and 24:0 LD conditions. Letters denote significant  
 647 differences in expression between groups. Expression is normalised counts of mRNA copies detected  
 648 via Nanostring nCounter.  
 649



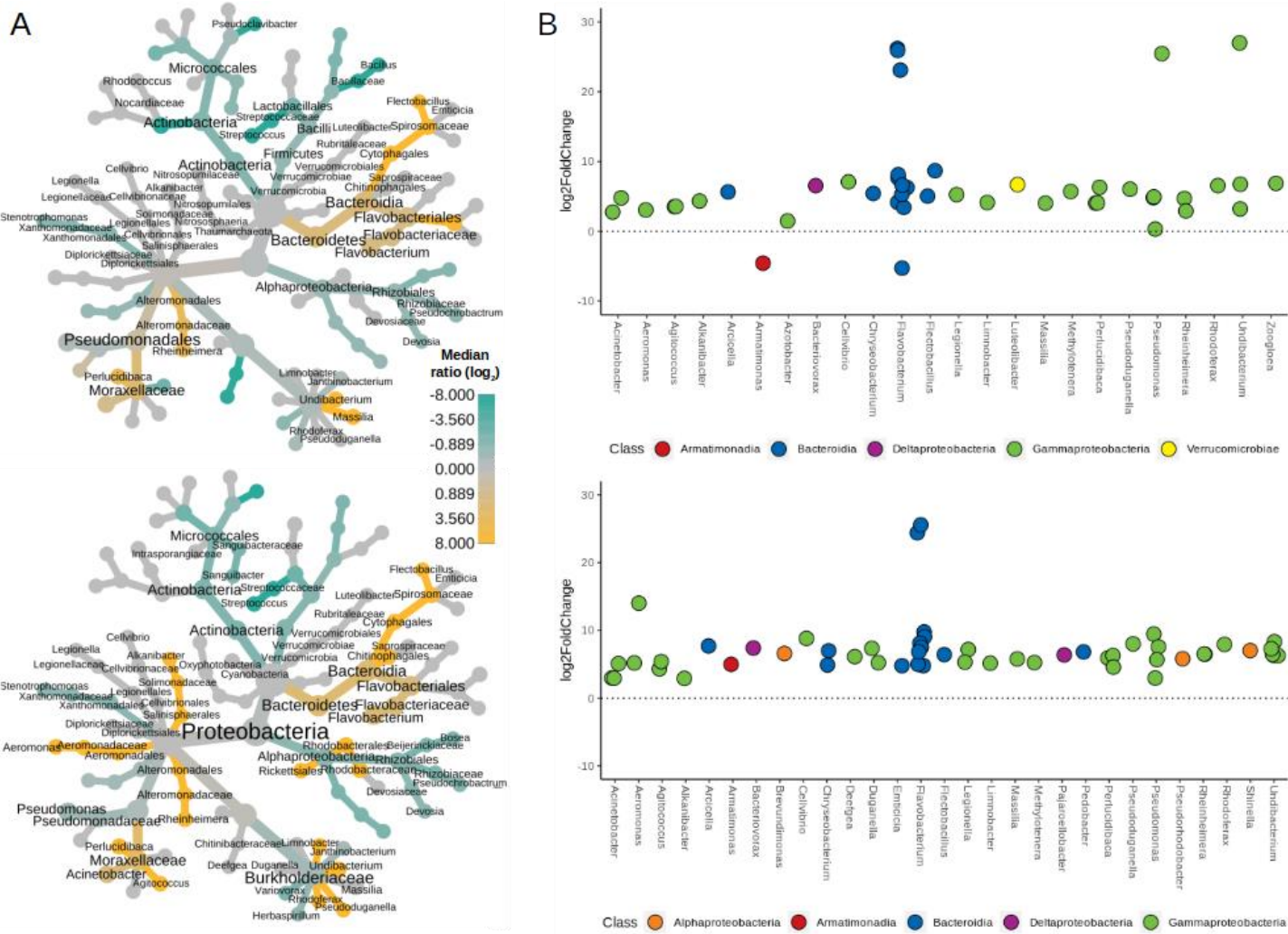
650

651 **Figure 2:** Mean expression ( $\pm 1$  S.E.) of core clock genes of uninfected (cyan) and *Argulus*-infected  
 652 (orange) rainbow trout maintained at 12:12 LD (left) and 24:0 LD (LL, right). Expression is  
 653 normalised counts of mRNA copies detected via Nanostring nCounter. Curves denote cosinor  
 654 waveform fitted using CircaCompare. Grey shading indicates time periods in darkness (grey dashing  
 655 indicates equivalent 12:12 LD light transitions on LL plots).



656

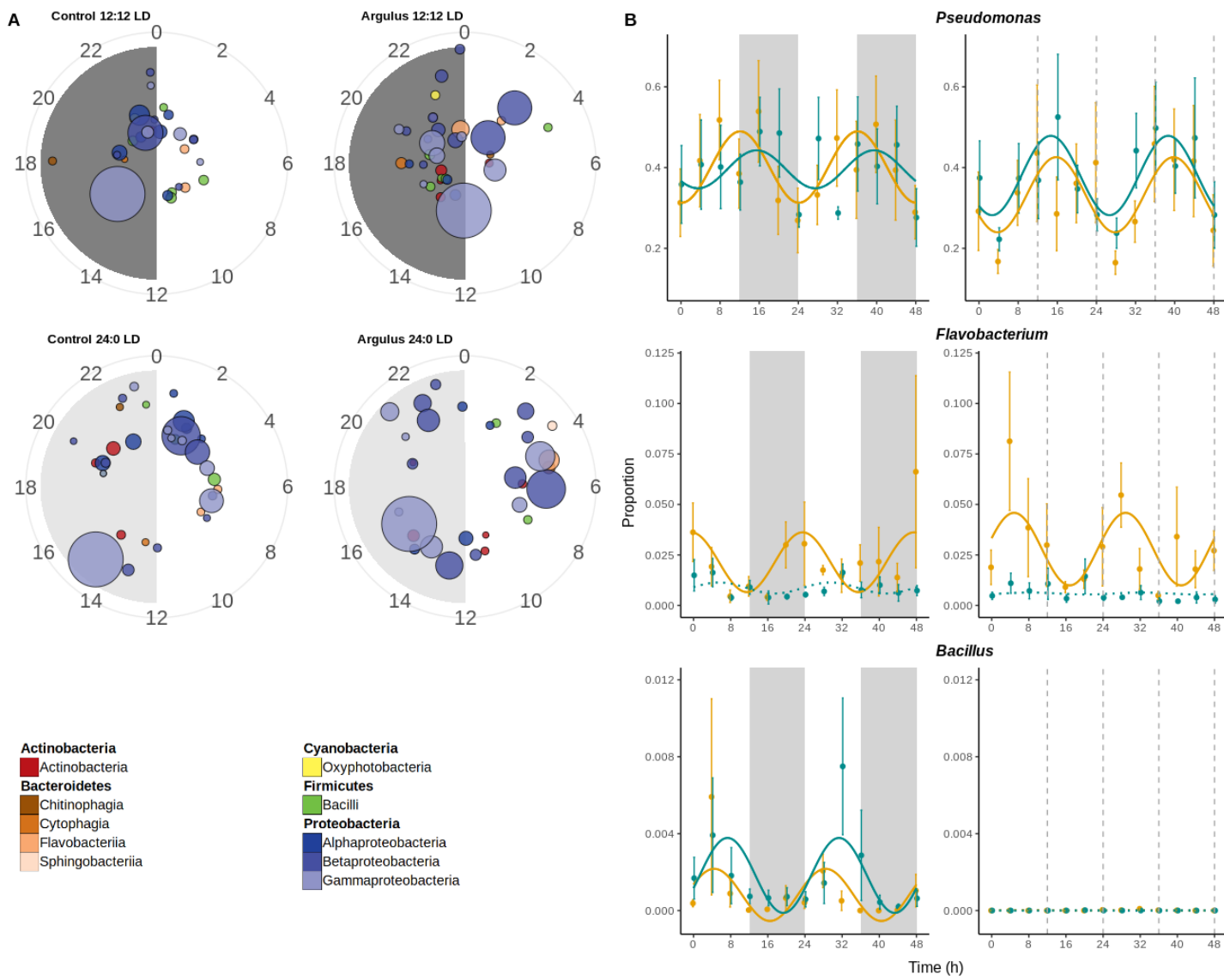
657 **Figure 3:** Alluvial plots of most abundant bacteria families (average >1% across all data) in healthy  
658 (A, C) and *Argulus foliaceus* infected (B, D) trout under 12:12 LD (A, B) and 24:0 LD (C, D)  
659 photoperiods. Horizontal bars indicate periods of light (white) and dark (black).  
660



661

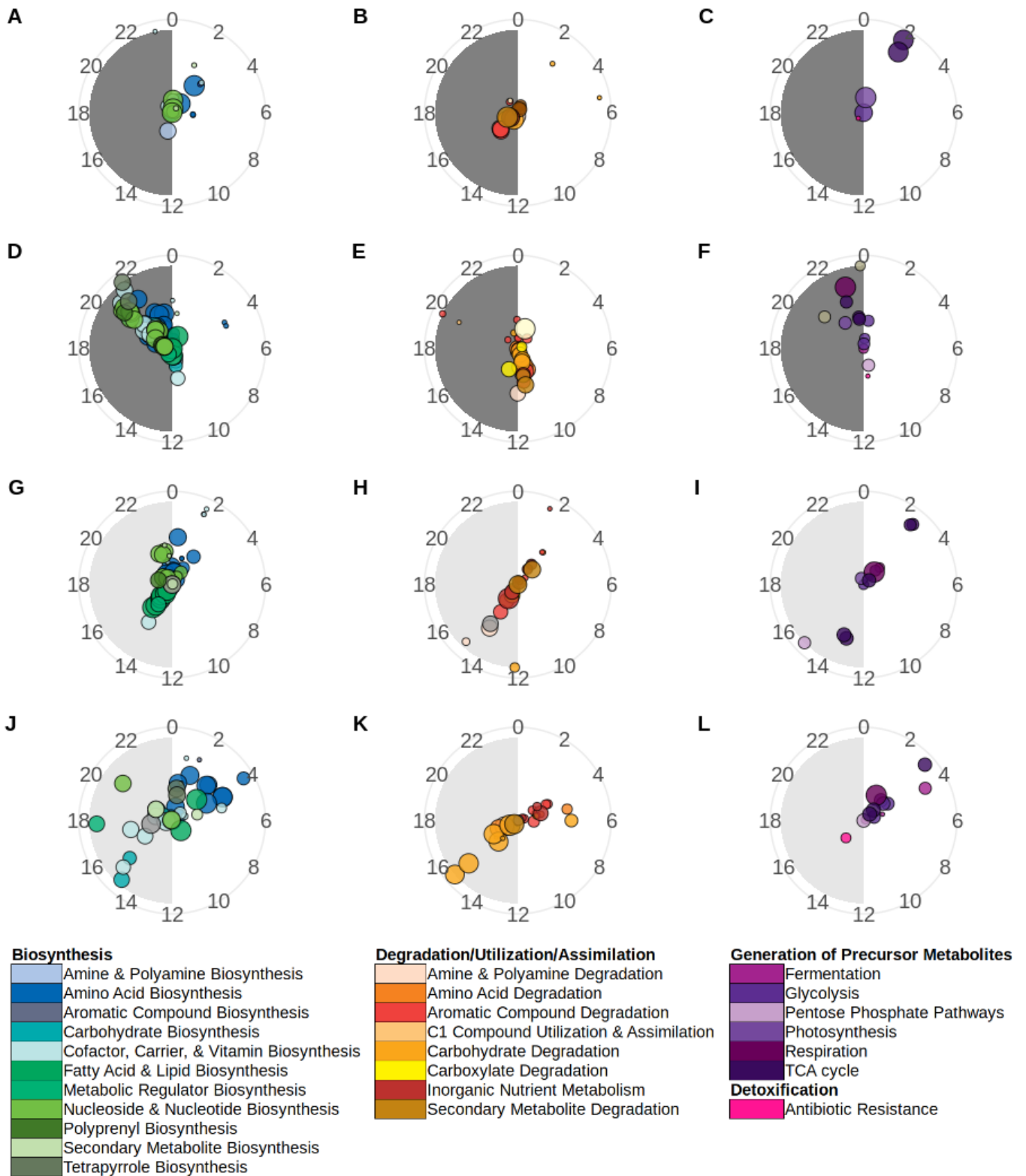
662 **Figure 4:** A) Heat trees contrasting bacteria taxa abundance between healthy and *Argulus foliaceus*  
 663 infected fish under 12:12 LD (top) or 24:0 LD (bottom) photoperiods. The colour of each taxon  
 664 represents the log<sub>2</sub> ratio of median proportions of reads. Taxa with significant differences are  
 665 labelled, determined using a Wilcox rank-sum test followed by a Benjamini-Hochberg (FDR)  
 666 correction for multiple comparisons. Taxa coloured cyan are enriched in healthy fish and those  
 667 coloured orange are enriched in infected fish. Node size is relative to prevalence in all samples. B)  
 668 Taxa with significantly different abundances (FDR-corrected p-value <0.05) between healthy and *A.*  
 669 *foliaceus* infected fish under 12:12 LD (top) or 24:0 LD (bottom) photoperiods, determined via  
 670 DESeq2 analyses. Taxa above the dotted line are significantly more abundant in infected fish, below  
 671 the line are more abundant in healthy fish.  
 672





673

674 **Figure 5:** A) Polar plots showing times of peak relative abundance of significantly rhythmic  
 675 microbiome genera. Each circle represents a genus, coloured by class and scaled by average relative  
 676 abundance. Radian indicates time of peak and distance from centre indicates significance (more  
 677 significant/stronger rhythms toward edge of plot). B) Examples of rhythmic bacteria genera (full  
 678 results presented in Table 3).  
 679



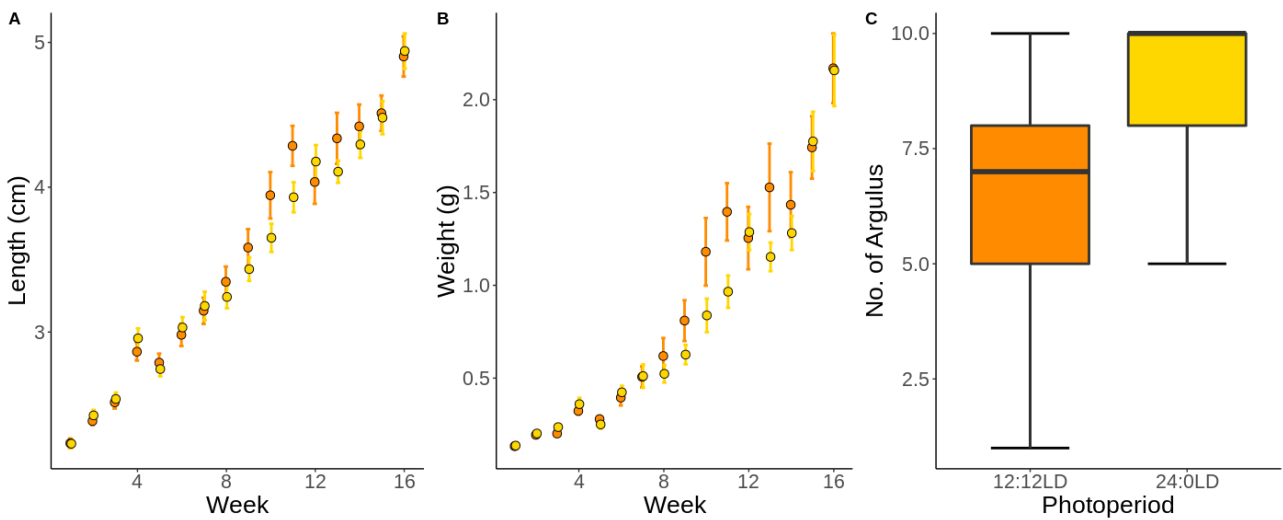
680

681 **Figure 6:** Polar plots showing peak relative abundance of significantly rhythmic microbiome  
 682 MetaCycle pathways. Each circle represents a pathway, coloured by MetaCycle class and sized by  
 683 average relative abundance. Pathway radian indicates time of peak and distance from centre indicates  
 684 significance (more significant/stronger rhythms toward edge of plot). Pathway identity determined  
 685 via Picrust2 and rhythmicity significance determined via eJTK\_cycle (Bonferoni-corrected P-values  
 686 <0.05). Circacompare was used to fit waveforms and determine estimates of rhythms peaks. A, B, C  
 687 = healthy trout under 12:12 LD. D, E, F = *Argulus*-infected trout under 12:12 LD. H, I, J = healthy  
 688 trout under 24:0 LD. K, L, M = *Argulus*-infected trout under 24:0 LD. Full details of pathways are  
 689 provided in Supplementary Datafile 1.

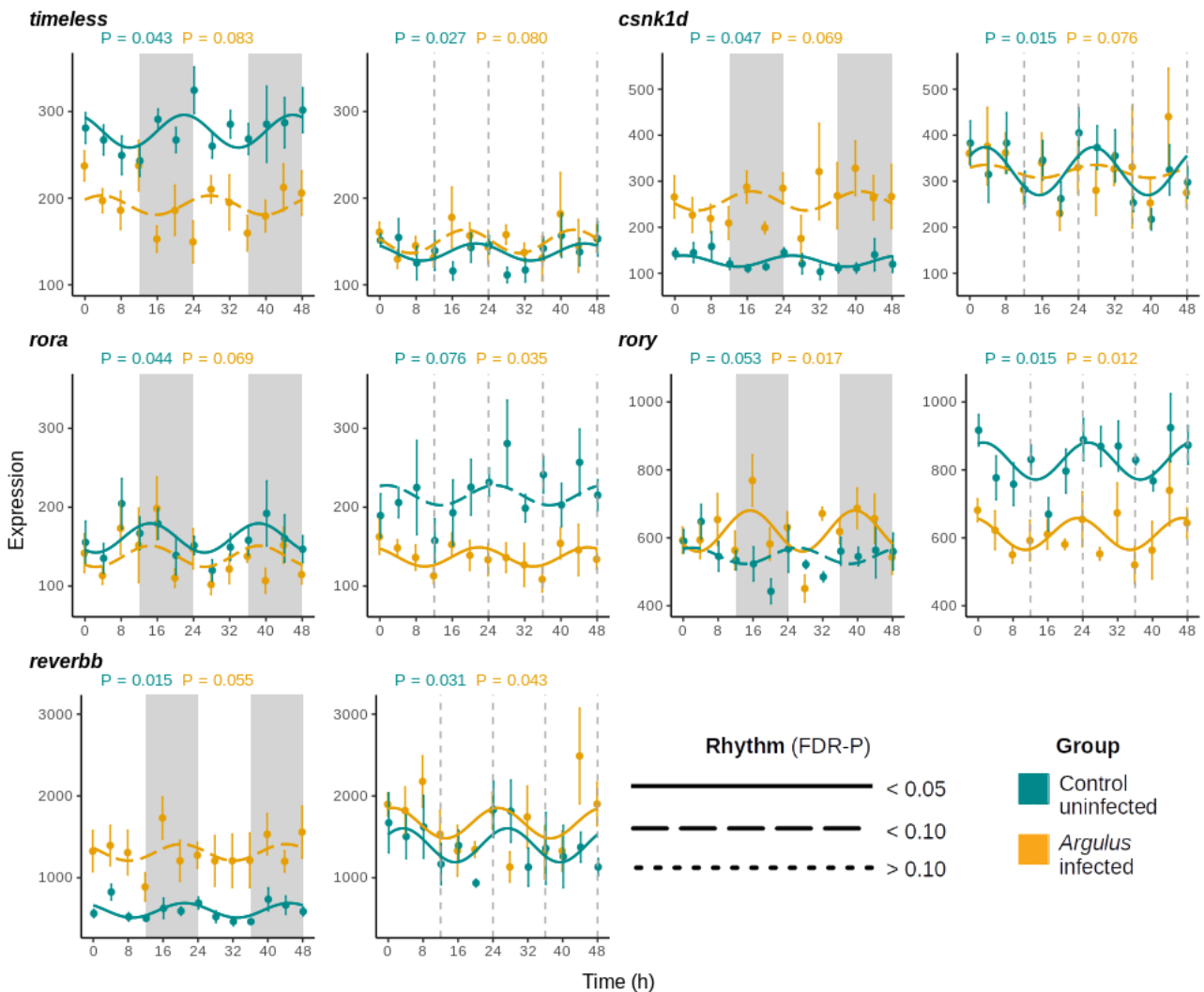


690

691 **Figure 7:** Co-occurrence networks of microbial genera (pink) and host gene expression (orange =  
 692 clock, green = immune, blue = corticotropin) in healthy (top) and *Argulus*-infected (bottom) trout  
 693 under 12:12 LD. Node and label size scaled to degree centrality score. Label colour denotes  
 694 rhythmicity (black = rhythm FDR p-value < 0.05, grey = rhythm FDR p-value > 0.05). Connection  
 695 colour indicates association (grey = positive, red = negative, determined by Spearman correlation  
 696 tests) and connection width scaled to correlation strength (thicker lines denote a higher correlation  
 697 coefficient).

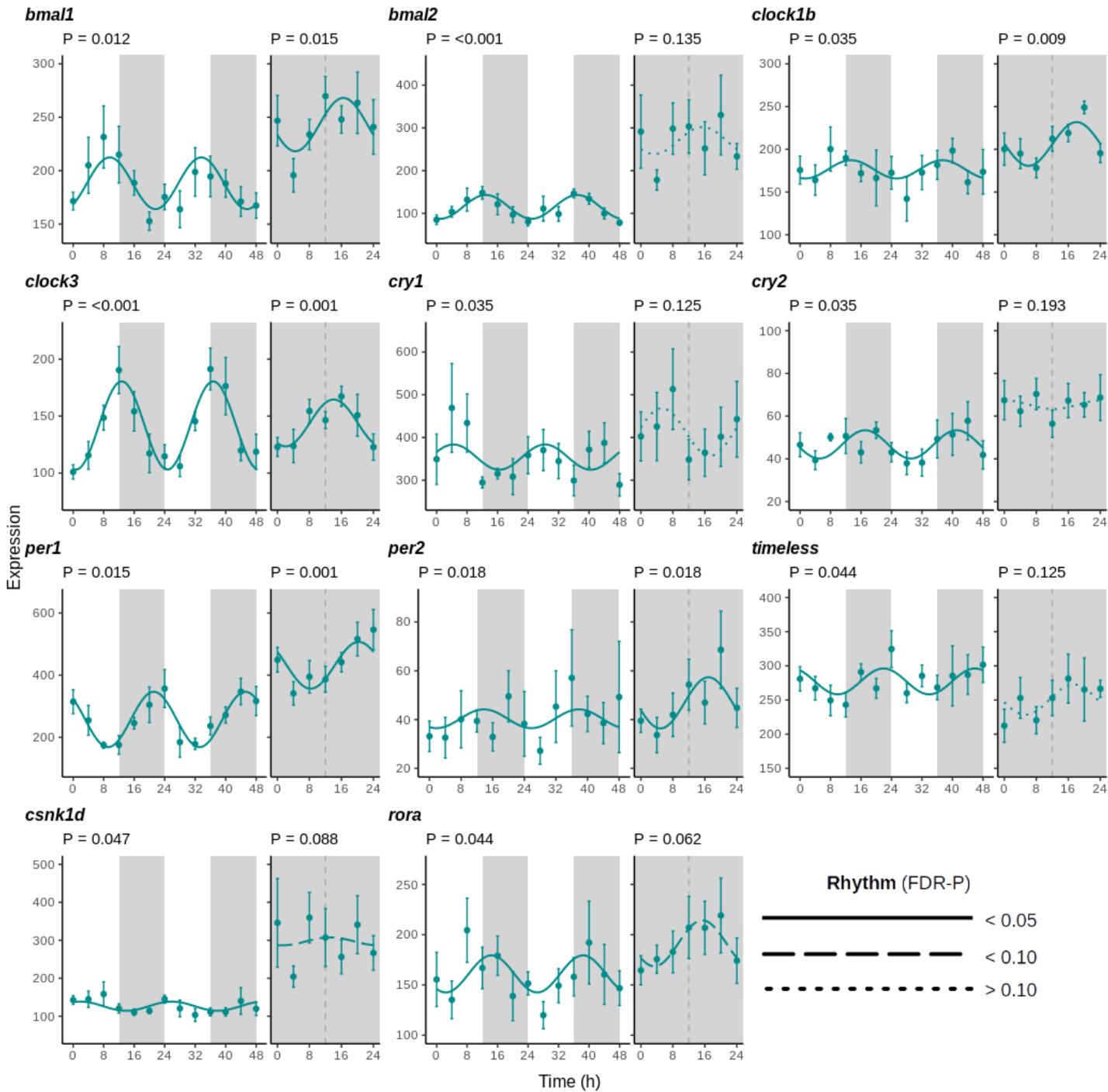


698  
699 **Supplementary Figure 1:** Average A) standard length and B) weight of trout ( $\pm 1$  S.E.) over 16-week  
700 growth trial under 12:12 LD (orange) and 24:0 LD (yellow). C) Boxplots of number of *Argulus*  
701 *foliaceus* lice infecting fish 7 days post-inoculation.  
702  
703



704  
705 **Supplementary Figure 2:** Mean expression ( $\pm 1$  S.E.) of accessory clock genes of uninfected (cyan)  
706 and *Argulus*-infected (orange) rainbow trout maintained at 12:12 LD (left) and 24:0 LD (LL, right).  
707 Expression is normalised counts of mRNA copies detected via Nanostring nCounter. Curves denote  
708 cosinor waveform fitted using CircaCompare. Grey shading indicates time periods in darkness (grey  
709 dashing indicates equivalent 12:12 LD light transitions on LL plots).

710



711

712

713

714

715

716

**Supplementary Figure 3:** Mean expression ( $\pm 1$  S.E.) of clock genes of rainbow trout under 12:12 LD and DD. Expression is normalised counts of mRNA copies detected via Nanostring nCounter. Curves denote cosinor waveform fitted using CircaCompare. Grey shading indicates time periods in darkness (grey dashing indicates subjective day-night transition in DD).



**Supplementary Figure 4:** Mean expression ( $\pm 1$  S.E.) of innate immune genes of uninfected (cyan) and *Argulus*-infected (orange) rainbow trout maintained at 12:12 LD (left) and 24:0 LD (LL, right). Expression is normalised counts of mRNA copies detected via Nanostring nCounter. Curves denote cosinor waveform fitted using CircaCompare. Grey shading indicates time periods in darkness (grey dashing indicates equivalent 12:12 LD light transitions on LL plots). Only genes with significant rhythm in one or more groups shown.



725

726

727

728

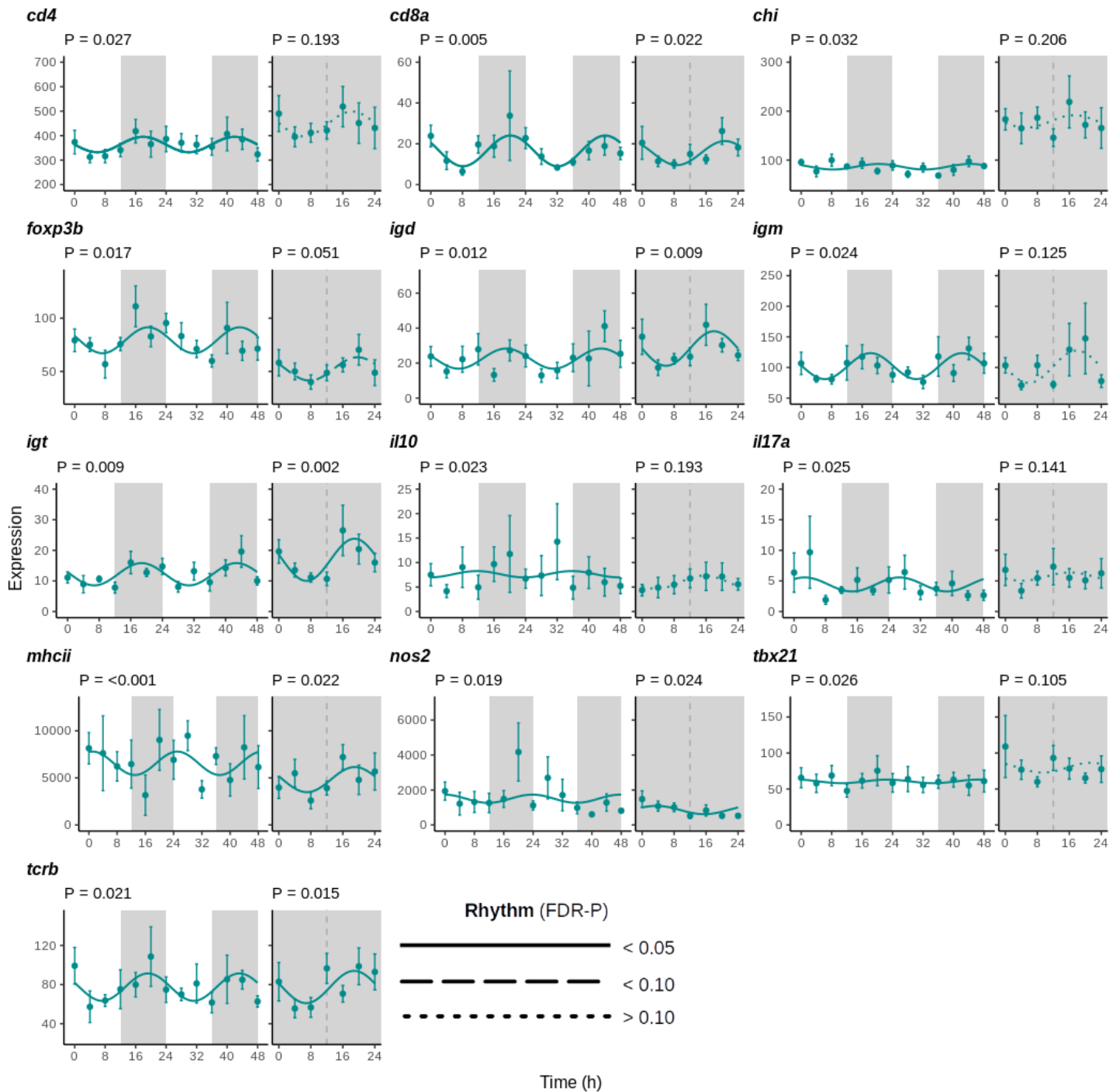
729

730

731

732

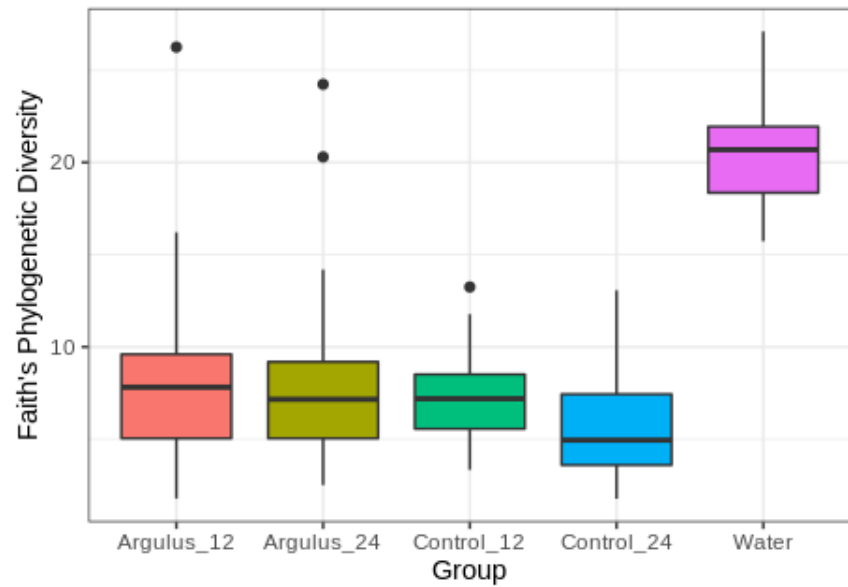
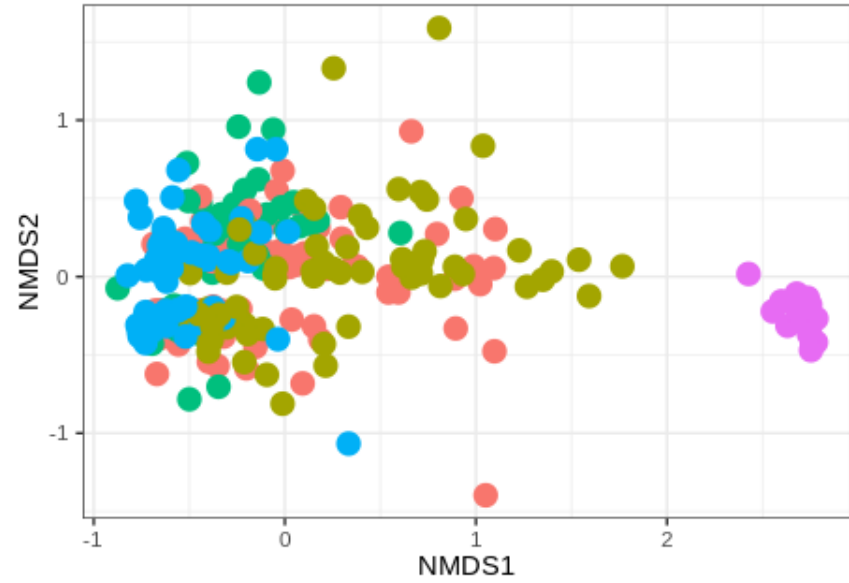
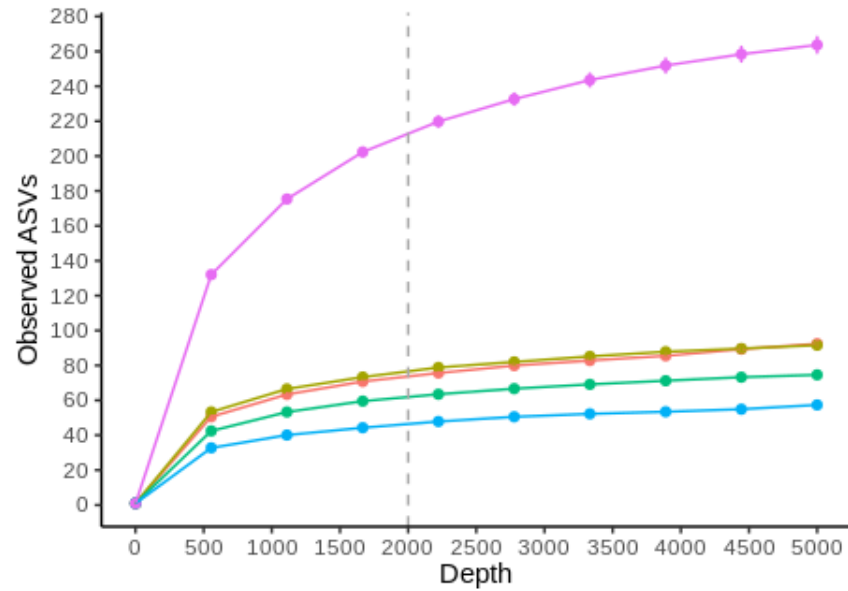
**Supplementary Figure 5:** Mean expression ( $\pm 1$  S.E.) of adaptive immune genes of uninfected (cyan) and Argulus-infected (orange) rainbow trout maintained at 12:12 LD (left) and 24:0 LD (LL, right). Expression is normalised counts of mRNA copies detected via Nanostring nCounter. Curves denote cosinor waveform fitted using CircaCompare. Grey shading indicates time periods in darkness (grey dashed indicates equivalent 12:12 LD light transitions on LL plots). Only genes with significant rhythm in one or more groups shown.



733  
734  
735  
736  
737  
738

**Supplementary Figure 6:** Mean expression ( $\pm 1$  S.E.) of immune genes of rainbow trout under 12:12 LD and DD. Expression is normalised counts of mRNA copies detected via Nanostring nCounter. Curves denote cosinor waveform fitted using CircaCompare. Grey shading indicates time periods in darkness (grey dashing indicates subjective day-night transition in DD).

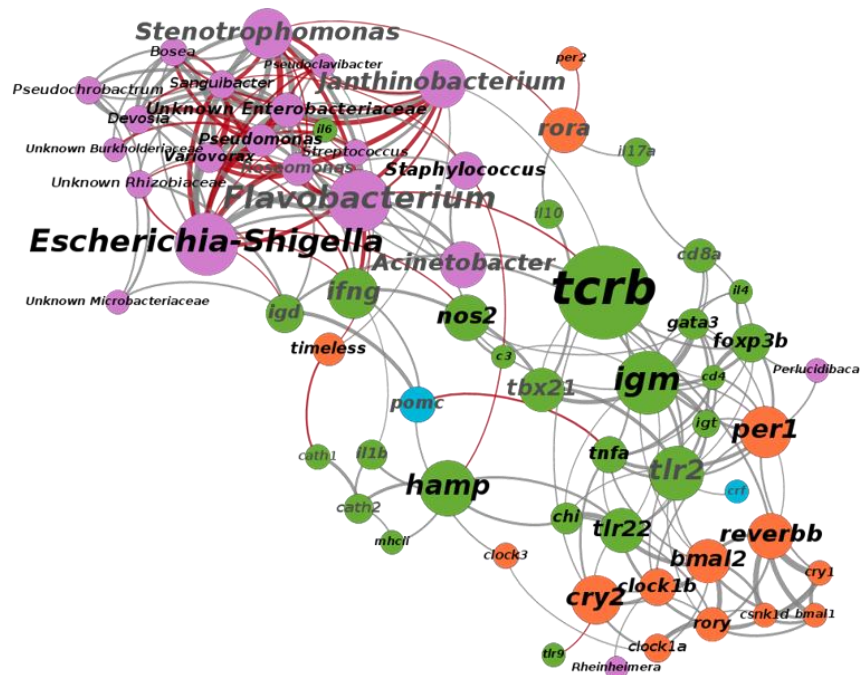




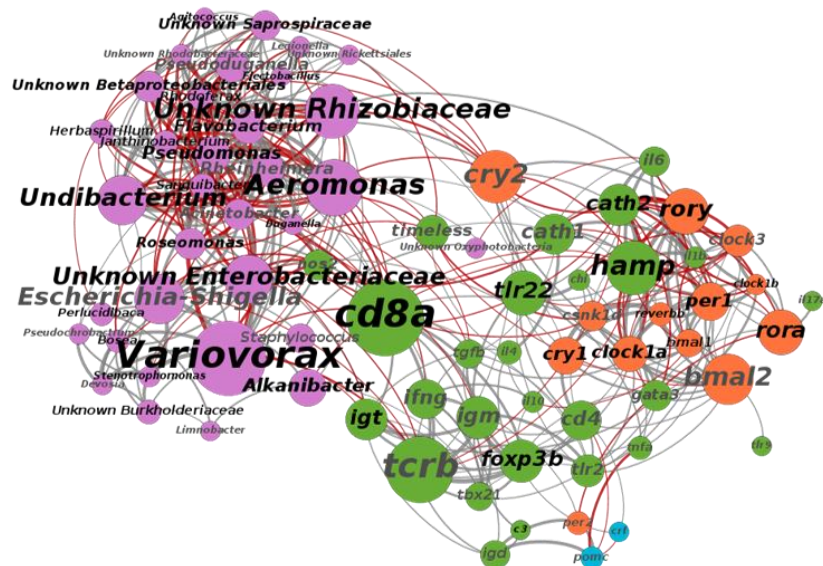
739  
740  
741

**Supplementary Figure 7:** A) Rarefaction plots of detected amplified sequence variants (ASVs) by sampling depth. B) NMDS ordination of microbiome profiles. C) Alpha diversity plots by treatment group.

A



B



742  
 743 **Supplementary Figure 8:** Co-occurrence networks of microbial genera (pink) and host gene  
 744 expression (orange = clock, green = immune, blue = corticotropin) in healthy (top) and *Argulus*-  
 745 infected (bottom) trout under 24:0 LD. Node and label size scaled to degree centrality score. Label  
 746 colour denotes rhythmicity (black = rhythm FDR p-value <0.05, grey = rhythm FDR p-value >0.05).  
 747 Connection colour indicates association (grey = positive, red = negative, determined by Spearman  
 748 correlation tests) and connection width scaled to correlation strength (thicker lines denote a higher  
 749 correlation coefficient).